General Disclaimer

One or more of the Following Statements may affect this Document

- This document has been reproduced from the best copy furnished by the organizational source. It is being released in the interest of making available as much information as possible.

- This document may contain data, which exceeds the sheet parameters. It was furnished in this condition by the organizational source and is the best copy available.

- This document may contain tone-on-tone or color graphs, charts and/or pictures, which have been reproduced in black and white.

- This document is paginated as submitted by the original source.

- Portions of this document are not fully legible due to the historical nature of some of the material. However, it is the best reproduction available from the original submission.

JANUARY 1978

Geosynchronous Microwave Atmospheric Sounding Radiometer (MASR) Feasibility Studies

Final Reports for MASR Feasibility Study Contract NAS 5-24082 and MASR Antenna Feasibility Study Contract NAS 5-24087

NASA Technical Officers
J Shiue
L R Dod
Hughes Program Managers
F E Goodwin
A T Villeneuve

Volume I Management Summary

HUGHES
HUGHES AIRCRAFT COMPANY
SPACE AND COMMUNICATIONS GROUP
AND
RADAR SYSTEMS GROUP

Hughes Ref No. D8647/D9236 • SCG 70531R

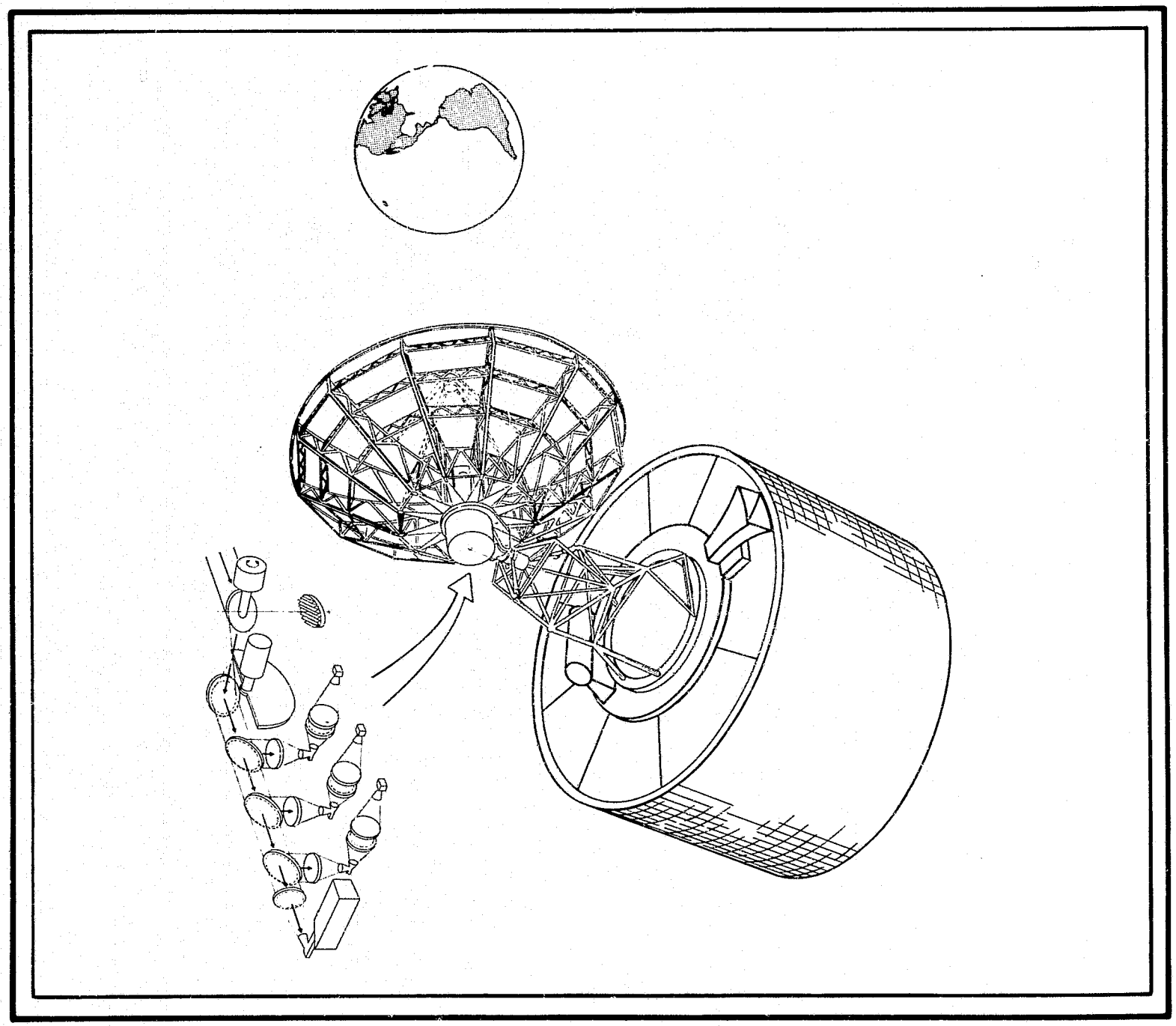

JANUARY 1978

Geosynchronous Microwave Atmospheric Sounding Radiometer (MASR) Feasibility Studies

Final Reports for MASR Feasibility Study Contract NAS 5-24082 and MASR Antenna Feasibility Study Contract NAS 5-24087

NASA Technical Officers
J Shiue
L R Dod
Hughes Program Managers
F E Goodwin
A T Villeneuve

Volume I Management Summary

HUGHES

HUGHES AIRCRAFT COMPANY
SPACE AND COMMUNICATIONS GROUP
AND
RADAR SYSTEMS GROUP

Hughes Ref No. D8647/D9236 • SCG 70531R

CONTENTS

1. INTRODUCTION TO MANAGEMENT SUMMARY

1. INTRODUCTION TO MANAGEMENT SUMMARY

The geosynchronous microwave atmospheric sounding radiometer (MASR) concept has great merit in meteorological applications. The radiometer instrument and antenna studies summarized in this report show that the concept is feasible.

The mission of the microwave atmospheric sounding radiometer (MASR) is to collect data to aid in the observation and prediction of severe storms. The geosynchronous orbit allows the continuous atmospheric measurement needed to resolve mesoscale dynamics. The instrument may operate in conjunction with multispectral imaging and infrared sounding sensors, and will be particularly valuable in collecting data in overcast regions. The anticipated ability to predict severe thunderstorms and larger cyclonic storms from MASR data adds to the economic and social benefit.

Angular resolution of MASR is limited by the beamwidth of a shuttle launched antenna (4.4 meter diameter) at the 118 and 183 GHz oxygen and water vapor sounding frequencies. Temperature resolution is a function of system noise temperature and integration time. Resolution element size and required integration time combine to limit the mapping coverage rate. From geosynchronous orbit, the 4.4 meter antenna provides nadir earth surface resolution of about 20 km at 183 GHz. The antenna is mechanically scanned in raster fashion to cover an area with contiguous resolution cells. The nominal dwell time per cell is 1 second at 183 GHz, allowing an area 800 by 800 km to be mapped in about 30 minutes.

Temperature sounding is achieved by obtaining a profile of the thermal radiance of the atmosphere in the frequency region of the 118 GHz oxygen absorption line. There are 11 double sideband (DSB) channels centered at the peak of this line and located various distances from the line center. Each channel will receive radiation predominately from a given altitude layer of the atmosphere, and the atmospheric temperature profile can be obtained from the 11 measured brightness temperatures using an inversion algorithm.

Similarly, there are six DSB channels centered at the 183 GHz water vapor line to determine the humidity profile. In addition, there are two window bands at 104 and 140 GHz to correct the measurements at 118 and 183 GHz for ground emissions (see Figures 1 and 2).

This document, Volume I - Management, summarizes the highlights of final reports on both the radiometer instrument and antenna studies. The radiometer instrument summary includes a synopsis of Volume II - Radiometer Receiver Feasibility, including design, recommended configuration, performance estimates, and weight and power estimates. The summary of the antenna study includes a synopsis of Volume III - Antenna Feasibility, including preliminary design tradeoffs, performance of selected design, and details of the mechanical/thermal design.

The radiometer study program has shown the feasibility of the radiometer receiver. It also reviews the technology status and suggests a point design for the four-band radiometer. The point design configuration features IMPATT local oscillators and balanced mixers on three of the bands and a TEO oscillator-doubler combination on one band. Radiometric ΔT performance of 0.21° is estimated on both the temperature and humidity sounding channels, which meets typical mission requirements. The package weighs 50 pounds and requires 81 to 98 watts to operate.

BAND	BANDWIDTH (IF)	CHANNELS	FUNCTION
183 GHz	10 GHz	6	WATER VAPOR ABSORPTION
140	1	1	WINDOW
118	4.1	11	OXYGEN ABSORPTION
104	1	1	WINDOW

70531-101

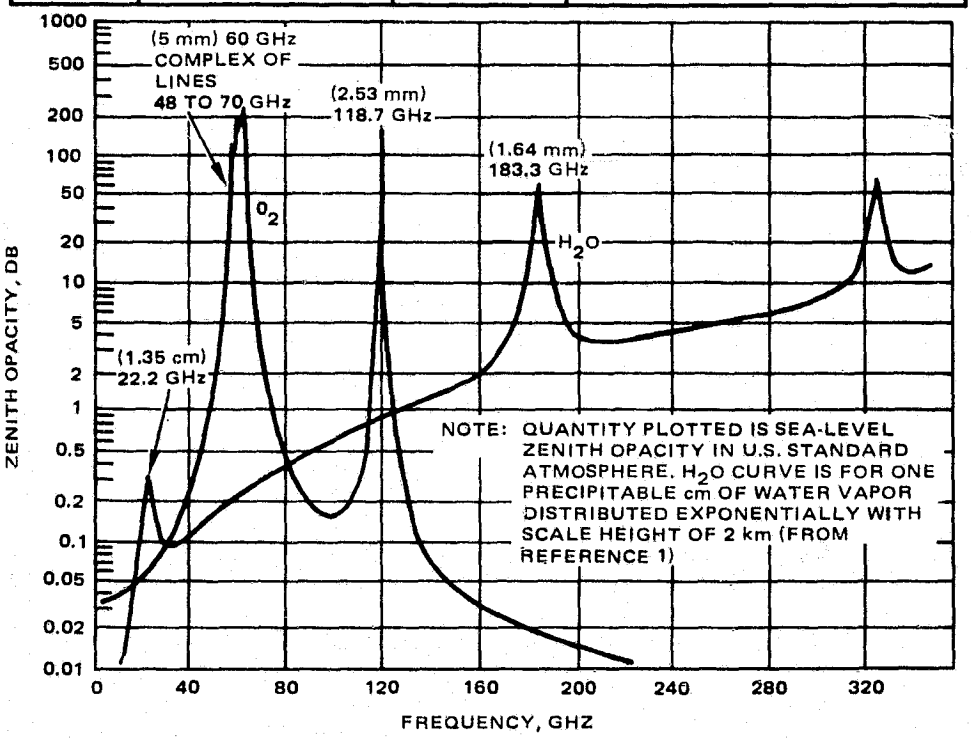

FIGURE 1. MICROWAVE ABSORPTION RESONANCES OF O_2 AND H_2O AVAILABLE FOR SOUNDING

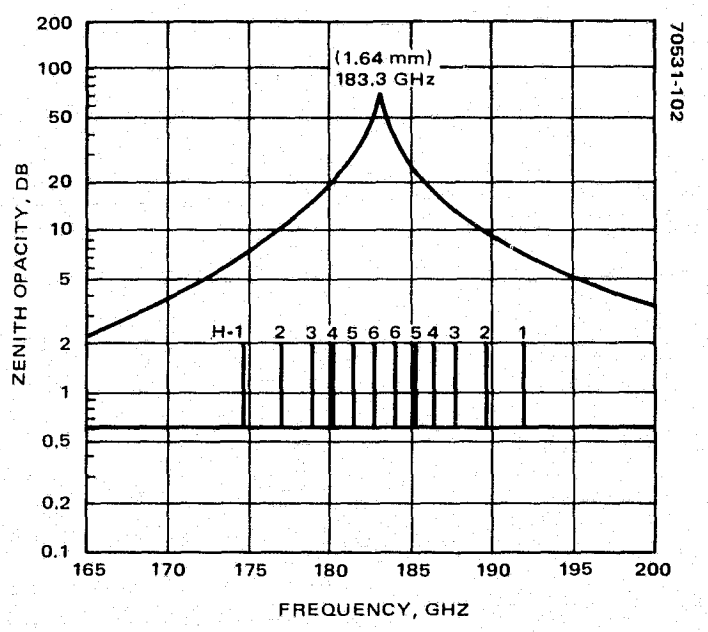

70531-102

FIGURE 2. H_2O SOUNDING CHANNELS H-1 TO H-6

The antenna brings all four frequency bands to a common focus. The radiometer receiver package is designed to demultiplex the four bands through the use of quasi-optical filters and to direct the individual beams to four separate feed horns, followed by four separate receivers. The 118 and 183 GHz receivers have very wide band channelized IF systems for the purpose of profiling the microwave spectrum of the atmosphere at these frequencies. Window bands measure the temperature of the earth's surface and each requires only one IF channel. A common chopper wheel and calibration load serve all four bands. Synchronous detection and other signal processing are achieved through a single onboard digital processor. Figure 3 is a simplified block diagram of the radiometer receiver subsystem.

The antenna study program reported in Volume III shows the advantages of the symmetrical cassegrain approach compared to an off-axis parabola in achieving high performance for the least stringent tolerances. A beam efficiency of 94.6 percent and maximum sidelobes of 33 dB below the principal maximum are estimated, assuming a perfect surface figure. The effects of an rms surface tolerance of 1.7 mils reduce the overall beam efficiency to 85 percent. Effects of blockage by the subreflector and struts reduce overall antenna efficiency by about 10 percent.

The antenna mechanical and thermal design was performed under subcontract by the General Dynamics Astronautics Division. Weight estimates of the complete antenna and gimbal with collapsible yoke are the order of 200 pounds if the assembly is constructed of GY-70/X-30 ISO graphite/epoxy composite.

Volume IV Appendix is devoted to theoretical comments on reference averaging and chopper frequency selection.

The authors are grateful to the following for their assistance in preparing this final report: D. H. Staelin, Massachusetts Institute of Technology; D. N. Held and A. R. Kerr, NASA-Goddard Institute of Space Sciences; T. S. Chu, Bell Telephone Laboratory; J. M. Schuchardt, J. B. Langley, and J. A. Stratigos, Georgia Institute of Technology; J. Payne, B. L. Ulich, National Radio Astronomy Observatory; and J. Shiue, L. King, and T. Dod, NASA Goddard Space Flight Center. Within Hughes, special thanks are given to the Technical Coordination Committee: T. A. Midford, K. L. Brinkman, P. Schwartz, W. H. Kummer, and Chairman R. Graves. Also, the technical assistance of P. Bernues, K. Weller, H. M. Endler, and E. L. Griffin proved to be invaluable.

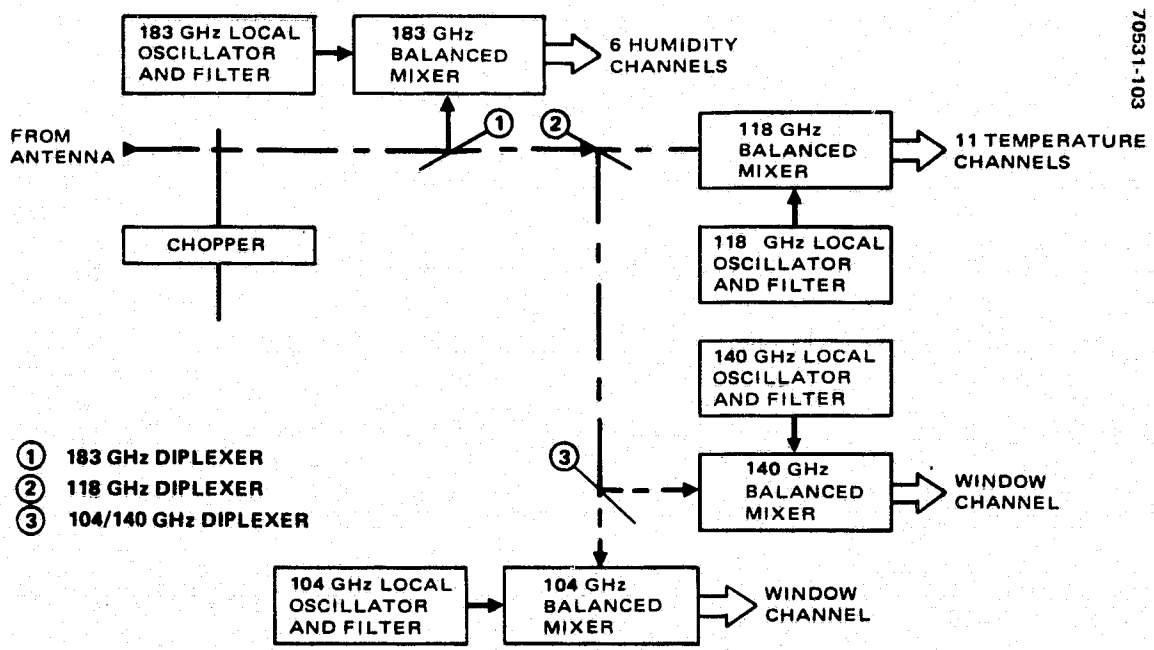

FIGURE 3. RADIOMETER RECEIVER SUBSYSTEM SIMPLIFIED BLOCK DIAGRAM

2. FOUR-BAND MILLIMETER WAVE RADIOMETER INSTRUMENT

2. Four-Band Millimeter Wave Radiometer Instrument

2.1 SUMMARY OF DESIGN REPORT

Design analyses and highlights of technical tradeoffs surrounding a radiometer configuration are described in this summary. Estimated ΔT's will meet anticipated MASR needs.

MASR study objectives are to make technical tradeoffs, determine feasibility, and isolate key technology areas. These objectives were achieved with in-depth technology surveys, concluding with a receiver hardware definition of sufficient detail to allow weight and power estimates and the preparation of a preliminary specification.

The study revealed the importance of quasi-optical techniques to reduce feed, diplexer circuit, and local oscillator (LO) filter losses. It also identified the mixer as the "softest" technology, including the mixer configuration, mixer diodes, mixer-to-IF impedance match, mixer bandwidth, and mixer local oscillator. While the best state of the art mixer performance was reported to be sufficient to meet MASR requirements, typical performance is in general marginal. Conclusions are that MASR is feasible, ΔT (radiometer temperature resolution) requirements generally can be achieved, quasi-optical design techniques are recommended, and mixer development methodology will pace the program.

Volume II consists of sections on Design Analysis, Receiver Design, and Antenna Interface; appendices deal with the MASR concept, and optical design formalism, reference averaging, and properties of materials. The following paragraphs summarize the highlights of each section of Volume II.

Design Analysis. Radiometer temperature resolution is commonly expressed as the minimum temperature difference which can be detected

$$\Delta T = KT_S/\sqrt{B\tau}$$

where

T_S = system noise temperature

B = IF bandwidth

τ = integration time

From system analysis of the radiometer, it was determined that the effective sensitivity factor K of the radiometer (normally K = 2 for a Dicke switched system) could be reduced to a value approaching 1.4, depending on the gain stability of the system, by using the technique of reference averaging. The improvement in temperature resolution results by integrating the reference channel over a number of pixel periods, where a pixel period equals the integration time of the signal channel. With practical limitations, improvement factor offered by reference averaging is about equivalent to that achievable with a double Dicke (Graham's receiver) system, but does not require the complexity of two receivers.

It is recommended that calibration of the radiometer receiver be performed at the antenna feed with a movable reflector that periodically switches the receiver input to a reference hot load and to cold space. The calibration accuracy expected is of the order of ±1°K in all channels. The radiometer system calibration, including the main antenna, must be performed in the far field of the main antenna. Possible methods of achieving total radiometer system calibration are discussed in Topic 5.4, Volume II.

It is recommended that quasi-optical filters be used both for LO filters and for frequency multiplexing in MASR. Analytical techniques commonly used for optical system design were found to be advantageous; ray matrices and Gaussian beam formalism provide an extremely versatile design approach for quasi-optics. Unconditional stability of the beam optical system assures negligible loss due to diffraction and radiation from these open structures. In Volume II, Appendix B provides the fundamental reference work of Kogelnik and Li which details the mathematical formalism; Topic 3.7 summarizes the work and illustrates its applications to quasi-optical systems.

Appendix C, Volume II presents an analysis that determines the effects of gain variation errors in a reference averaging radiometer and the maximum improvement achievable. This analysis shows that for typical gain stability the K value can be reduced from K = 2 (Dicke case with square wave modulation and demodulation) to K = 1.4. The analysis is summarized and results presented in Topic 3.4 of Volume II.

A theoretical treatment of reference averaging was conducted which includes general considerations of chopping frequency, asymmetrical chopping, and chopper transition effects. Because this work is highly theoretical and lengthy, it is included in Volume IV of this report.

Another theoretical treatment was developed of chopper frequency selection in a reference averaging Dicke radiometer. One of the more significant results is that second detector low frequency noise (1/f), which is suppressed in a conventional Dicke radiometer by proper selection of chopper frequency, cannot be suppressed in the same way in a reference averaged system. Rather, the reference averaged system has a floor on the detector noise feedthrough. Because this analysis is highly theoretical and lengthy, it is also included in Volume IV.

Receiver Design. A tentative receiver subsystem block diagram is shown in Figure 1. The basic four-band radiometer receiver consists of a quasi-optical quadraplexer which separates the bands and directs the beams to separate feed horns and mixers. The 118 and 183 GHz mixers are matched into IF networks that provide IF channel separation for the 11 temperature channels and six water vapor channels. The window bands at 104 and 140 GHz are amplified after mixing over nominal IF bandwidths of about 1 GHz and detected. A signal processing and control subsystem manages all functions, including the antenna drive, calibration control, chopper synchronization, and synchronous detection of the 19 radiometer channels. In addition, the signal processing and control subsystem provides the capability to perform reference averaging to enhance the performance of the radiometer.

Radiometer temperature resolution or ΔT performance is a direct function of system noise temperature. To facilitate the following discussion, the contributing factors are given in Table 1, together with example values for parameters for each radiometer band and a computation of its respective system noise temperature.

Mixer Tradeoff. The heart of the radiometer receiver is the low noise mixer. Reported mixer conversion loss and noise temperature data are scattered over a wide range of values for the frequencies of interest. It is obvious that consistent mixer performance will be achieved only with great effort. A recommended approach is to begin mixer development early and to build a selected inventory of mixers suitable for MASR.

The quality of mixer performance is conventionally expressed in terms of single-sideband noise temperature T_{MSSB} and mixer conversion loss L_M. Mixer performance is affected by the quality of the mixer diode material, precision contacting, microwave circuit design, and impedance match for both the signal

TABLE 1. CONTRIBUTORS TO T_{SYSTEM}

$$T_{SYSTEM} = T_A + (L_F - 1)\, T_O + L_F\, T_R$$

$$T_R = \frac{1}{2}\,(T_{MSSB} + L_M\, T_{IF})$$

T_R = double sideband receiver temperature
T_A = antenna temperature
L_F = feed loss
T_O = feed temperature
L_M = mixer conversion loss
T_{IF} = IF noise temperature
F_{IF} = IF noise figure

70532-105T

System	183 GHz	140 GHz	118 GHz	104 GHz
T_A, °K	250	250	250	250
L_M, dB	8.5	6.5	5.0	5.0
F_{IF}, dB	5.0	3.0	3.5	3.0
T_{MSSB}, °K	2100	1100	600	600
$L_M\, T_{IF}$, °K	4438	1288	1135	910
T_R, °K	3269	1169	867	755
L_F, dB	0.5	1.0	1.0	1.0
$(L_F\text{-}1)\, T_O$, °K	35	70	70	70
T_S, °K	3952	1823	1412	1270

BAND	BANDWIDTH (IF)	CHANNELS	FUNCTION
183 GHz	10 GHz	6	WATER VAPOR ABSOPTION
140	1	1	WINDOW
118	4.1	11	OXYGEN ABSORPTION
104	1	1	WINDOW

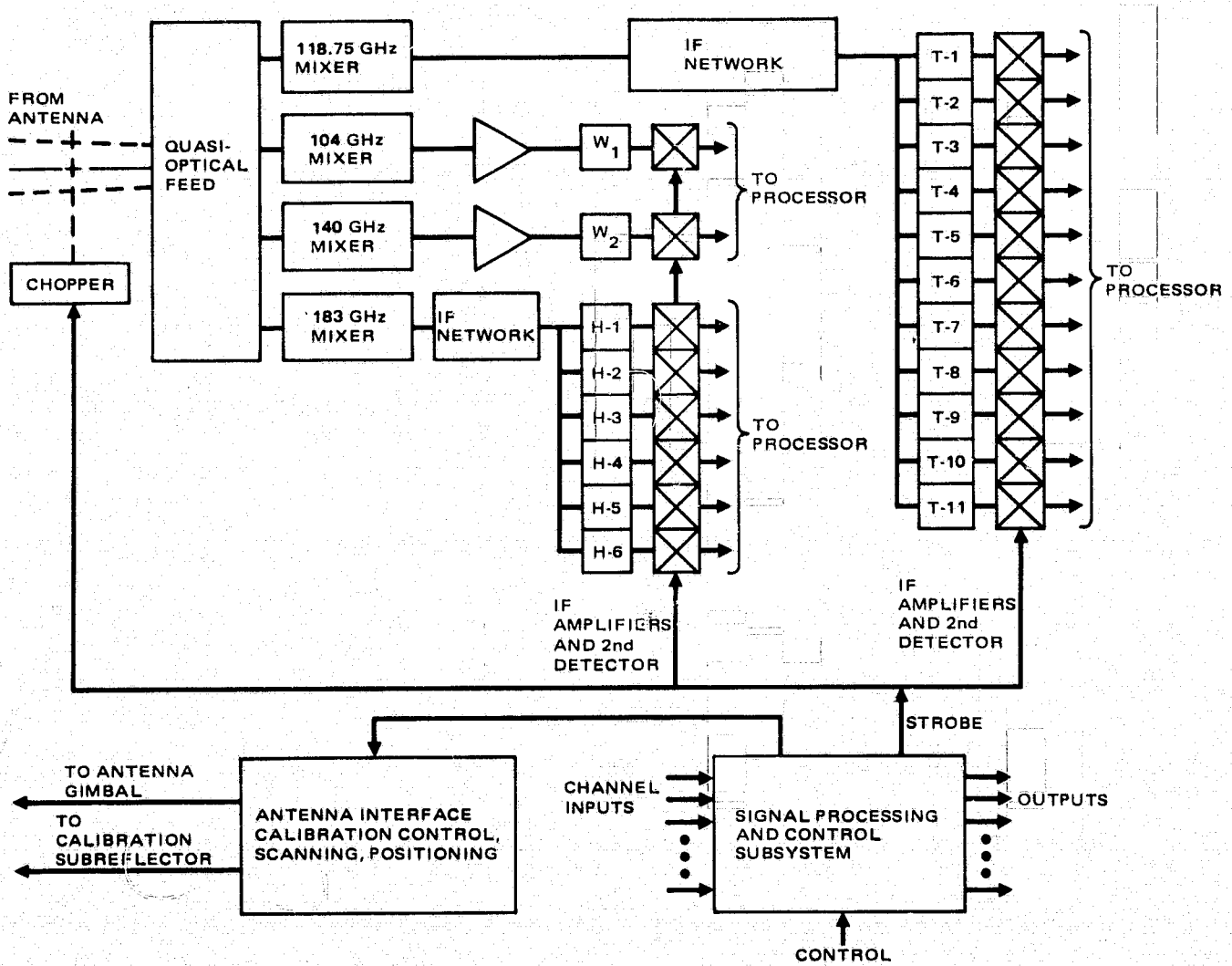

FIGURE 1. FOUR CHANNEL MICROWAVE H_2O AND O_2 SOUNDING RADIOMETER TENTATIVE BLOCK DIAGRAM

input and IF output circuits. Further, it is also a function of the quality and level of local oscillator signal. Of all the factors influencing the radiometer system noise temperature, T_{MSSB} is the term over which there is least control. State of the art values of T_{MSSB} reported in the literature vary over a wide range. Figure 2 shows a number of demonstrated values. The solid line shows the probable minimum achievable values expected, and also represents approximate MASR needs for the more difficult bands.

Balanced mixers have the desirable property of canceling LO noise and are recommended for MASR to provide a degree of immunity to the noise generated by solid state LO sources such as IMPATTS. Waveguide balanced mixers are the recommended baseline design. However, conventional balanced mixers at these frequencies are difficult to build. Subharmonically pumped mixers, a form of balanced mixer, also have LO noise cancellation properties. Further, these devices have the advantage of using a local oscillator at half the signal frequency.

Quasi-Optical Balanced Mixer. This study has produced an alternate approach to achieving the noise cancellation effects of a balanced mixer with two single-ended mixers in a quasi-optical assembly (Figure 3). The signal from the antenna is diplexed with a wire grid polarizer 1 and the 183 GHz band is reflected by 90°. The signal polarization is upward (not shown in figure) while the local oscillator polarization is in the plane (see Figure 3). Both signal and local oscillator encounter a rotation plane of 45° and are split by a second wire grid polarizer 2 and directed to separate single-ended mixer mounts. The signal and LO fields are in phase in one mixer and out of phase in the other. Their electrical outputs combine in such a way as to cancel the dc and noise terms while the IF terms add in phase. This approach was determined to be unique and was reported as a new technology item.

Local Oscillator Sources. It was determined that IMPATT and Gunn solid state sources are available for use as local oscillators. IMPATTS produce sufficient power in all four bands but are noisy and must be filtered with about 40 dB of filtering over each band of frequencies, which for the 183 GHz humidity band is ±10 GHz from the center frequency. The basic approach to accommodating the IMPATT is to utilize balanced mixers, that provide about 20 dB of immunity to the noise, and Fabry Perot quasi-optical filters that provide at least another 25 dB of filtering. The combined effects of the balanced mixer and quasi-optical filter provide sufficient margin to assure that a good low noise mixer is achieved.

The Gunn oscillator (or the transferred electron oscillator) is somewhat quieter than an IMPATT, but has an upper frequency limit near 100 GHz. With noise characteristics lower than that of an IMPATT and adequate power below 100 GHz, the Gunn oscillator is an attractive alternative to the IMPATT when used with a doubler or with a subharmonic mixer.

Local Oscillator Filters. Because of relatively high unloaded Q, Fabry-Perot quasi-optical filters have fundamental advantages over waveguide filters for selectivity and suppression of LO noise in the IF sidebands. Of the two types demonstrated, the parallel plate Fabry-Perot has the advantage of arbitrarily large rejection bands, while the ring configuration offers a unique LO injection scheme. Because of the wide IF bandwidth requirements however, the recommended filter for MASR local oscillators is the parallel plate configuration. Specific parallel plate filter designs were developed for each of the MASR bands.

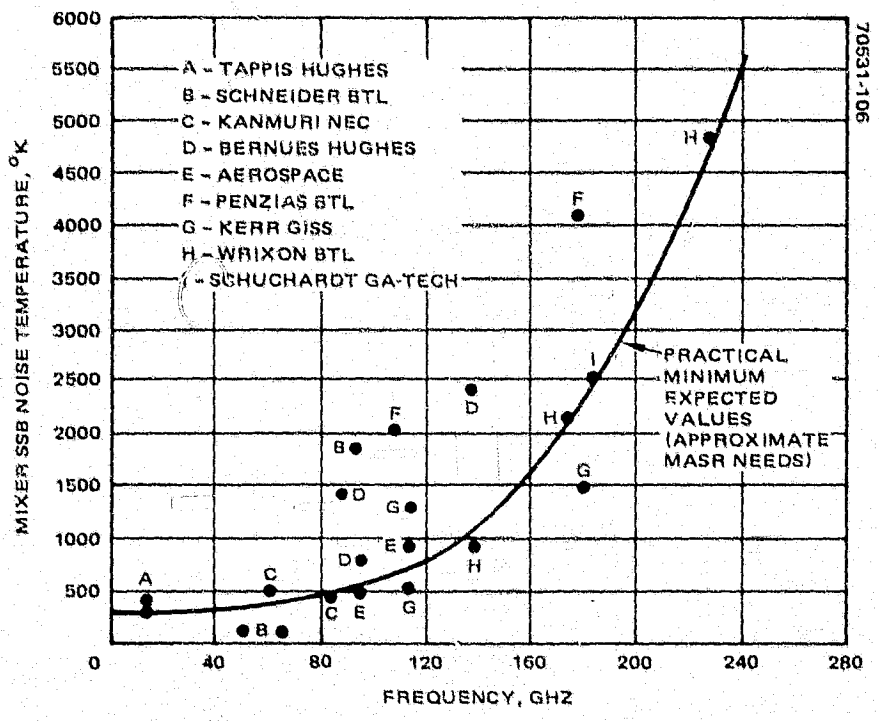

FIGURE 2. DEMONSTRATED LOW NOISE MIXER PERFORMANCE

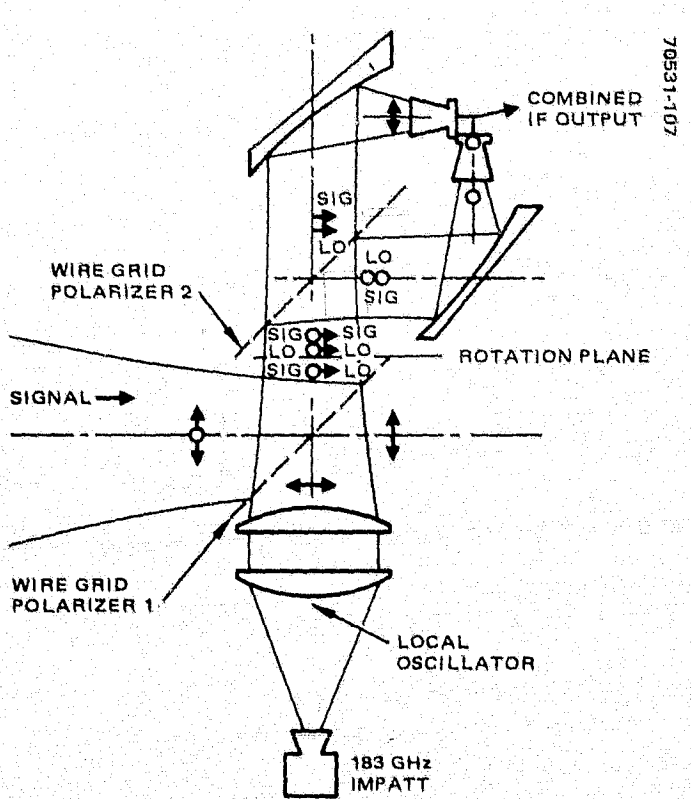

FIGURE 3. QUASI-OPTICAL BALANCED MIXER

The most difficult filter is that for the 118 GHz band which needs a loaded Q of 6000 to accommodate a minimum IF frequency of only 20 MHz. For a 118 GHz minimum IF frequency of 50 MHz instead of 20 MHz, a loaded Q of 2400 would be adequate, resulting in LO filter losses of 4.1 dB instead of 8.1 dB. The 118 GHz LO power is marginal with 8.1 dB filter loss, and raising the minimum 118 GHz IF would eliminate this problem.

IF Design. Difficult requirements for MASR are the 0.6 to 10 GHz IF network for the H_2O band and the 20 to 4000 MHz IF network for the O_2 band. Two approaches were analyzed; one utilizes available components and techniques while the other assumes the development of contiguous filter banks. The analyses show that while both approaches are feasible and technically suitable, the conventional approach requires less development. In either case, the ultimate performance of the IF network will be determined by how well the mixer-to-IF impedance match is maintained over the required bandwidth.

Antenna Interface. The antenna interface consists of an RF interface, thermal/mechanical interface, and calibration interface. In a typical antenna, the RF interface is defined by a waveguide that connects the receiver to the antenna feed. In the recommended quasi-optical design, the RF interface is defined by the complex beam parameters for the four bands. The illumination patterns for the individual bands are generated separately and combined in the quasi-optical quadraplexer.

The calibration interface deserves special comment. The calibration procedure for the radiometer receiver is self-contained. A positionable mirror at the antenna feed allows the receiver to look at the antenna, cold space, or a calibrated reference "hot" load. This two-point receiver calibration sequence could be performed in a few seconds and repeated often, allowing the receiver to measure antenna temperature T_A to an accuracy of about 1°K.

Knowing T_A accurately is only one step in obtaining mesoscale temperature data since the value of T_A is a function of the antenna beam efficiency, sidelobes, field brightness, and ohmic losses. The ultimate calibration of the actual target temperature against T_A is a difficult task which must be carefully performed in space. Topic 5.4 is devoted to the discussion of antenna calibration.

Quasi-Optical Antenna Feed. The tradeoff study shows that feed, diplexing, and LO filter losses could be significantly reduced by using quasi-optical components rather than waveguide components. Typically, a ten-fold reduction in losses is illustrated in the radiometer point design. Appropriately, optical design techniques are found to be powerful aids in achieving low loss designs of quasi-optical devices and systems. A novel quasi-optical feed was disclosed (Figure 4) which separates the 183 GHz channel with a wire grid polarizer (element 1) and separates the 118 GHz channel from the window channels with either a Fabry-Perot or resonant grid optical filter (element 2). The antenna feed point is imaged at each of the four horns. Typical feed losses, including 0.25 dB for each horn, are given in Figure 4.

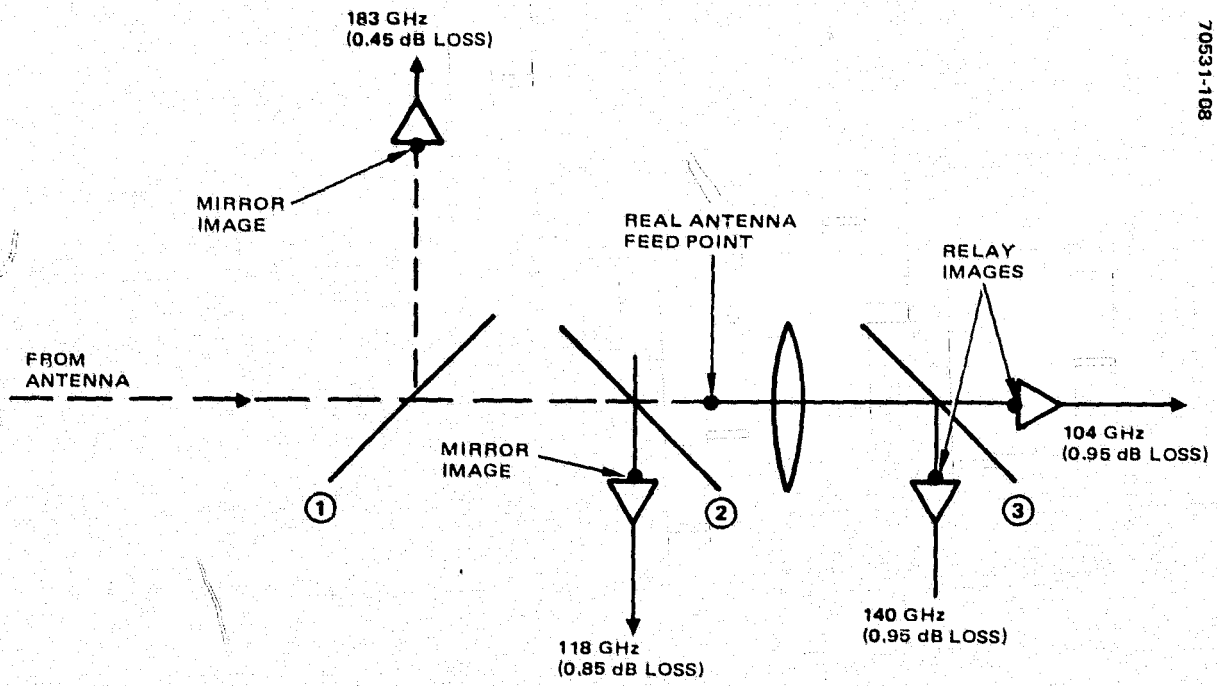

FIGURE 4. QUASI-OPTICAL FEED SCHEMATIC

2.2 RECOMMENDED RADIOMETER CONFIGURATION

The present study effort has resulted in the selection of an overall configuration which offers excellent theoretical performance and affords the least technical risk.

Millimeter wave technology status offers several approaches to MASR, each having "softness" but all are currently under rapid development. A preferred technical approach is difficult at present, but several configurations can meet MASR requirements. The study effort has resulted in the selection of a tentative configuration which appears to have least technical risk. Technology advances in alternate approaches could change the selection but the present design serves as a model to estimate weight, power, size, and cost of the flight instrument.

The baseline approach utilizes balanced mixers in all bands. IMPATT local oscillators with quasi-optical filters are recommended for 118, 140, and 183 GHz bands, while a TEO oscillator/doubler is recommended for the 104 GHz band. Quasi-optical demultiplexers are recommended in the form of band dropping mirrors for the 183, 140, and 118 GHz bands. These dropping mirrors are either wire grid polarizers, resonant grid dichroic mirrors, or Fabry-Perot filters. An isometric view of the optomechanical assembly is shown in Figure 1. The incoming beam from the antenna reaches a minimum beam waist at the calibration subreflector mirror, then focussed sharply to the chopper plane and recollimated by a matched off-axis mirror. The beam is formed and directed through a series of band dropping mirrors and to the balanced mixers for each band. The local oscillator signals are combined with the signal and IF outputs are directed to respective IF networks.

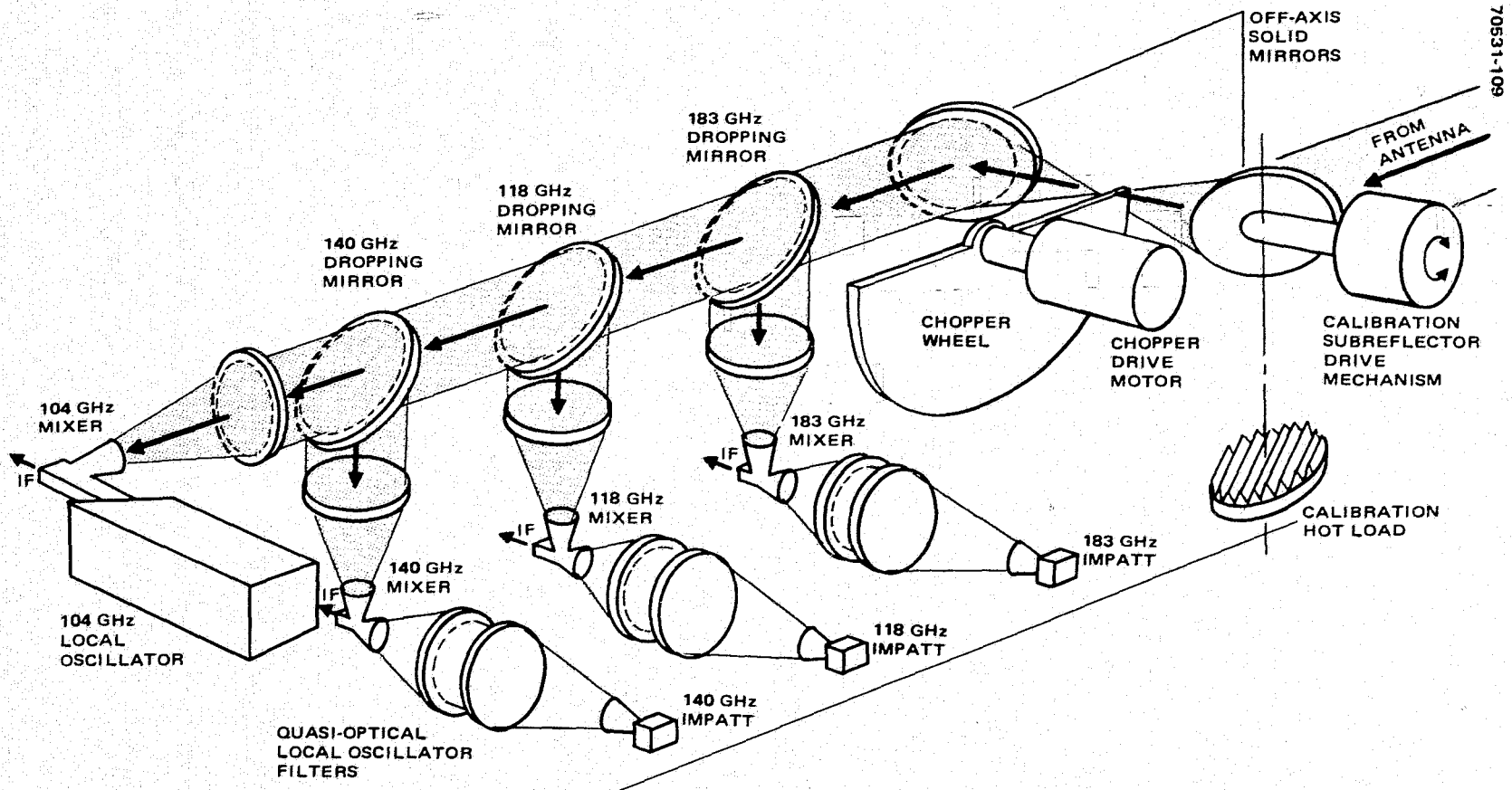

FIGURE 1. MASR OPTOMECHANICAL ASSEMBLY - ISOMETRIC VIEW

2.3 PERFORMANCE ESTIMATES

Tables 1 through 3 are performance estimates for the four radiometric bands based on state of the art technologies with modest improvements anticipated.

TABLE 1. PERFORMANCE ESTIMATES FOR 118 GHz BAND

Channel Number	f_{IF}, MHz	B_{IF}, MHz	F_{IF}, dB	T_{IF}, °K	ΔT		
					Goal	Dicke (K = 2)	Reference Average (K = 1.4)
T-1	3590	1000	3.3	330	0.2	0.06	0.04
T-2	1930	700	3.3	330	0.2	0.08	0.06
T-3	1140	400	3.5	359	0.2	0.11	0.08
T-4	740	287	3.5	359	0.2	0.14	0.10
T-5	490	212	3.5	359	0.2	0.16	0.11
T-6	315	137	3.0	290	0.2	0.18	0.13
T-7	200	92	3.0	290	0.2	0.22	0.16
T-8	125	57	3.0	290	0.2	0.27	0.19
T-9	80	32	2.5	225	0.2	0.34	0.24
T-10	52.5	22	2.5	225	0.2	0.40	0.29
T-11	30	22	2.5	225	0.2	0.40	0.29
Average					0.2	0.21	0.15

Center frequency	118.75 GHz
Mixer	Waveguide balanced
Mixer temperature, T_{MSSB}	1100°K
Mixer conversion loss, L_m	5 dB
Local oscillator	IMPATT
Local oscillator filter	Fabry-Perot parallel plate
Total IF bandwidth	19 to 4090 MHz
IF filter	Triplexer/9 way power divider
Feed loss	1 dB
Antenna temperature	250°K
Integration time	1.55 sec

70532-110T

TABLE 2. PERFORMANCE ESTIMATES FOR 183 GHz BAND

Channel Number	f_{IF}, GHz	B_{IF}, GHz	F_{IF}, dB	T_{IF}, °K	ΔT		
					Goal	Dicke (K = 2)	Reference Average (K = 1.4)
H-1	8.625	2.5	5.5	738	0.2	0.18	0.13
H-2	6.25	2.5	5.1	648	0.2	0.16	0.11
H-3	4.375	1.25	5.3	692	0.2	0.24	0.17
H-4	3.125	1.25	4.9	606	0.2	0.22	0.16
H-5	1.875	1.25	4.3	490	0.2	0.19	0.14
H-6	0.9375	0.625	3.7	389	0.2	0.24	0.17
			Average		0.2	0.21	0.15

Center frequency	183.30 GHz
Mixer	Waveguide balanced
Mixer temperature, T_{MSSB}	2100°K
Mixer conversion loss, L_m	8.5 dB
Local oscillator	IMPATT
Local oscillator filter	Fabry-Perot parallel plate
IF bandwidth	0.625 – 10 GHz
IF filter network	Cascaded diplexers
Feed loss, L_F	0.5 dB
Antenna temperature, T_A	250°K
Integration time	1.0 sec

70532-111T

TABLE 3. PERFORMANCE ESTIMATES FOR 104 AND 140 GHz BANDS

Channel Number	f_{IF}, MHz	B_{IF}, MHz	F_{IF}, dB	T_{IF}, °K	ΔT		
					Goal	Dicke (K = 2)	Reference Average (K = 1.4)
W-1	500	1000	3.0	290	0.2	0.05	0.04
W-2	500	1000	3.0	290	0.2	0.08	0.06

W-1 center frequency	104 GHz
W-2 center frequency	140 GHz
Mixers	Waveguide balanced
Mixer temperature, T_{MSSB}	
W-1	600°K
W-2	600°K
Mixer conversion loss, L_m	
W-1	5 dB
W-2	6.5 dB
Local oscillator	
W-1	Gunn doubler
W-2	IMPATT
Local oscillator filter	
W-1	Waveguide
W-2	Fabry-Perot parallel plate
Total IF bandwidth, each band	1 GHz
Feed loss, each band	0.95 dB
Antenna temperature, T_A	250°K
Integration time	
W-1	1.76 sec
W-2	1.31 sec

70532-112T

2.4 MECHANICAL SUBSYSTEM

The mechanical subsystem is designed to be accommodated in the main dish structure of the antenna. The receiver assembly is contained in a package 16 by 16 by 32 inches.

The receiver mechanical assembly includes a structural frame, pivoted mirror for calibration, chopper wheel, hot reference load, demultiplexer, and the four radiometer receivers. Suggested layouts are shown in Figures 1 and 2. The pivoted calibration mirror is shown in position to illuminate the subreflector of the antenna. The mirror is also capable of pointing at the hot reference load and at cold space. The chopper wheel assembly is shown in greater detail in Figure 2. The mirror is an off-axis parabola, bringing the incoming beam from the antenna to a sharp focus at a point where the chopper wheel intersects the beam. The beam waist at focus is 3.6 mm to the 99 percent truncation points. Since the chopper wheel circumference is about 300 mm, the chopper rise and fall transition ratios are given by

$$R_{RISE/FALL} = \frac{3.6}{150} = 2.4\%$$

Another parabolic segment is matched to the pivoted calibration mirror in such a way as to minimize aberrations. The beam is recollimated and directed to the quasi-optical demultiplexer and then to the separate mixers. Figure 1 shows the use of IMPATTS as local oscillators for three bands and a Gunn for the fourth band to illustrate the two available options. Access to the main antenna focus is through a cylindrical space 24 inches in diameter and 36 inches deep (Figures 3 and 4). The surface of the main parabola is provided with a 25 cm diameter circular hole that allows the beam from the antenna to come to focus at a point 16 cm behind the parabolic surface. When located in position, the pivoted subreflector of the receiver lies approximately at the focus of the antenna. A hole will be located in the antenna structure to allow the pivoted calibration subreflector to look at cold space.

The receiver mechanical subsystem occupies only one quadrant of the available space in the rear of the antenna, although the structure extends several inches into the other quadrants to accommodate a symmetrical axial beam.

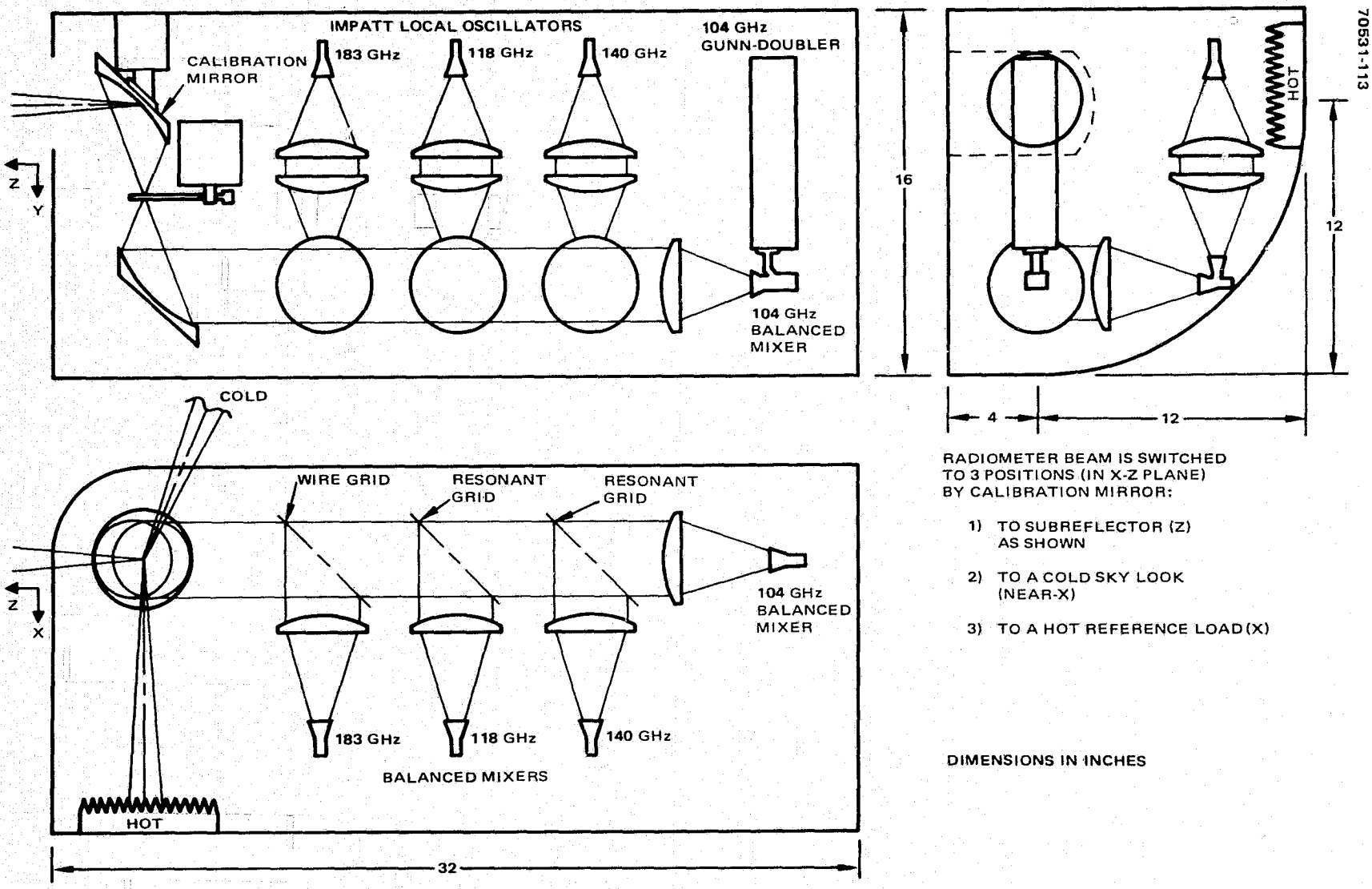

RADIOMETER BEAM IS SWITCHED TO 3 POSITIONS (IN X-Z PLANE) BY CALIBRATION MIRROR:

1) TO SUBREFLECTOR (Z) AS SHOWN
2) TO A COLD SKY LOOK (NEAR-X)
3) TO A HOT REFERENCE LOAD (X)

DIMENSIONS IN INCHES

70531-113

FIGURE 1. RADIOMETER MECHANICAL SUBSYSTEM

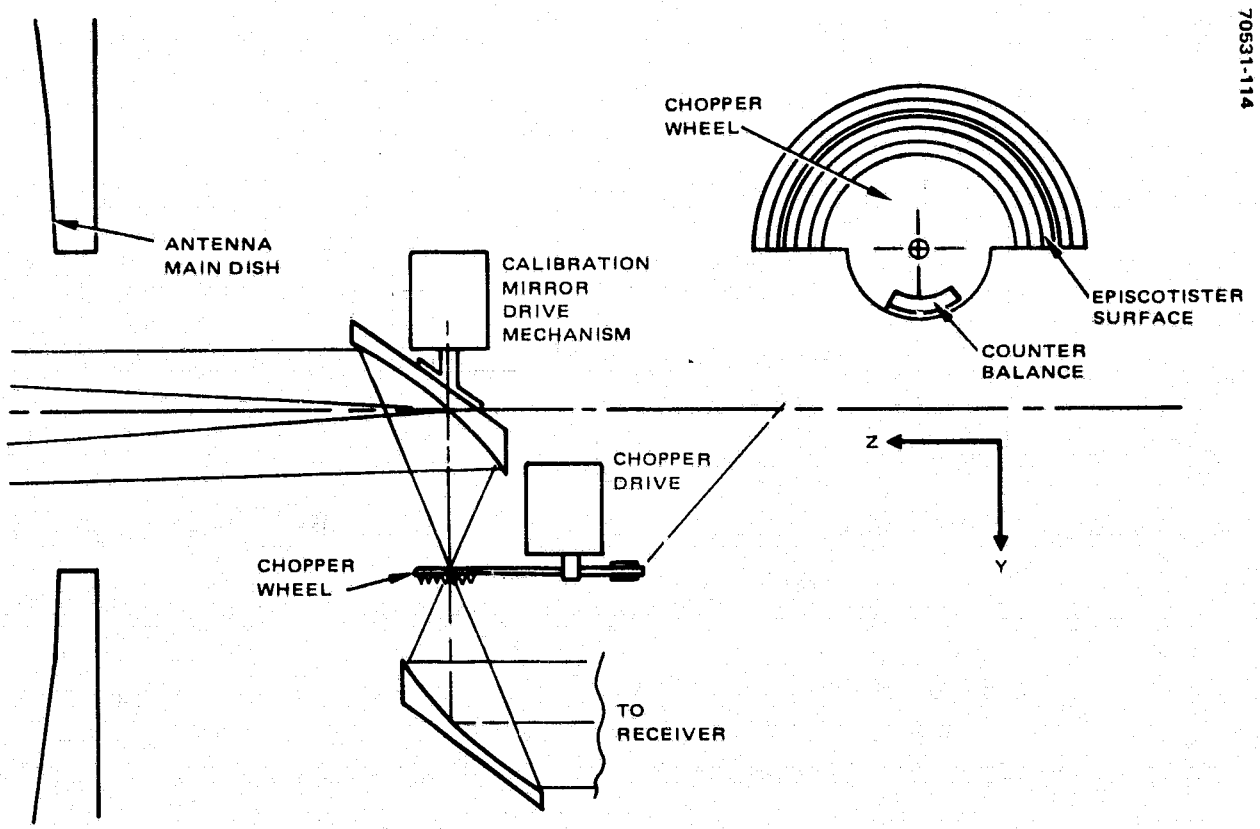

FIGURE 2. CALIBRATION MECHANISM AND CHOPPER WHEEL, TOP VIEW

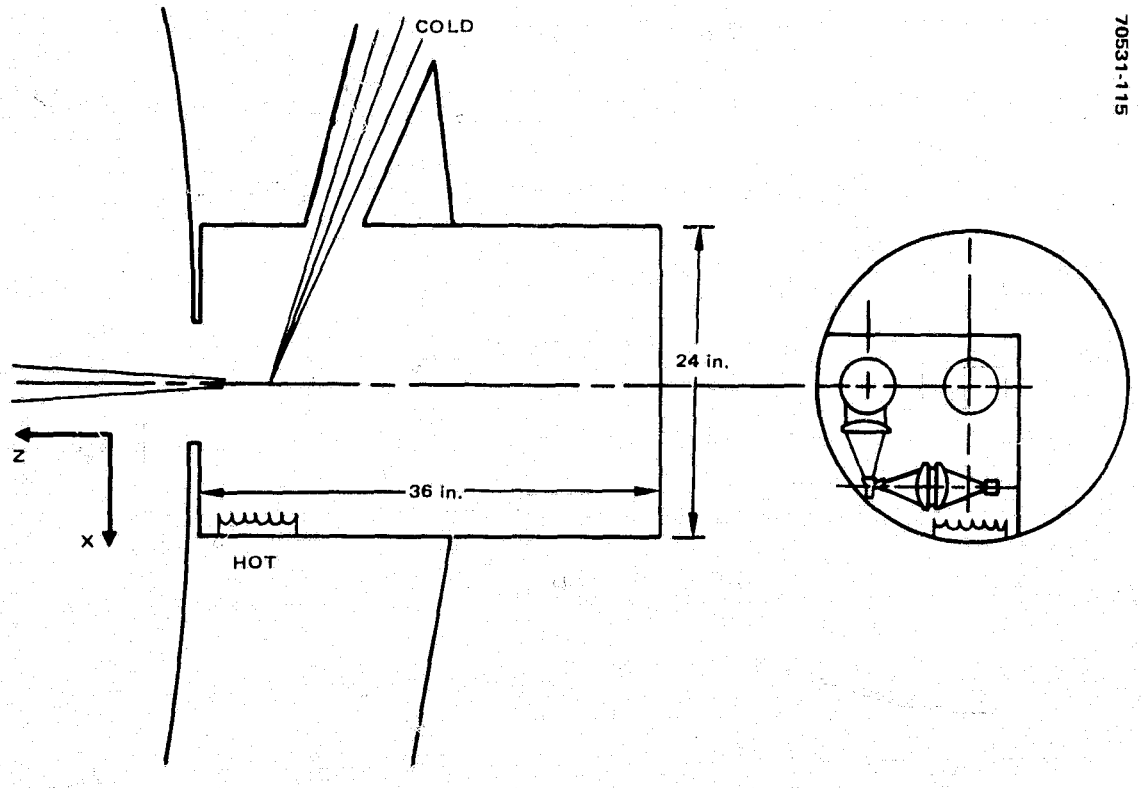

FIGURE 3. APERTURE FOR LOCATION OF RADIOMETER

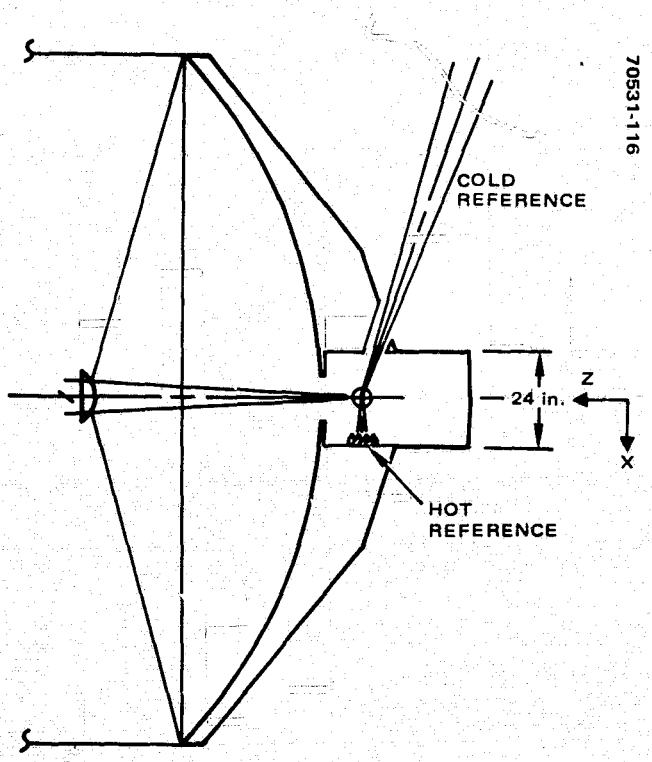

FIGURE 4. ANTENNA SIDE VIEW SHOWING
RADIOMETER CALIBRATION LOADS

2.5 WEIGHT AND POWER REQUIREMENTS

The weight, power, and thermal/mechanical interface data of the MASR payload are tabulated in Table 1.

TABLE 1. PAYLOAD WEIGHT AND POWER REQUIREMENTS

Weight Tabulation, lb		
Optomechanical subsystem	15.5	
183 GHz receiver subsystem	4.2	
118 GHz receiver subsystem	3.7	
104/140 GHz receiver subsystem	1.8	
Signal processing subsystem	1.0	
Miscellaneous electronics	1.4	
Cables and connectors	4.6	
Chassis	18.0	
Total MASR weight estimate, lb	50.2	
Power Tabulation, W		
Chopper drive	5	
Calibration mirror drive	15	0
Local oscillator sources	45.3	
IF amplifiers	3.2	
Signal processing	13.2	
Power conditioning	16.3	14.3
Total power required, W	98.0 max	81.0 min
Package Dimensions, in.	16 x 14 x 32	
Thermal Load, W	81 to 98	

70532-117T

3. 4.4 METER DIAMETER SYMMETRICAL CASSEGRAIN ANTENNA

3. 4.4 Meter Diameter Symmetrical Cassegrain Antenna

3.1 PRELIMINARY DESIGN TRADEOFFS

The criteria of performance, technical risk, development cost, and time favors the selection of a symmetrical cassegrain antenna over an off-axis antenna.

This section summarizes the study results of antenna systems capable of operating with a multichannel microwave radiometer for the 1984-85 time period. The size of the antenna is fixed at 4.4 meters diameter by resolution requirements and Shuttle launch capabilities. Two main antenna system candidates were compared: a paraboloidal reflector with an offset focal point feed and a symmetrical cassegrain reflector system (Figure 1). The beam efficiency of both candidates appear to be acceptable, provided stringent mechanical tolerances (Table 1) on feed position and reflector surface can be met. From the point of view of maintaining the required positional accuracies and surface tolerances, as well as manufacturability, cost effectiveness, and technical risk, the symmetrical cassegrain was selected as the preferred configuration (see Table 2). The main performance characteristics have been calculated, and a mechanical design study has been conducted to provide estimates of the technical risk, costs, and development time required for the construction of such an antenna system. The system consists of a reflector, a two-axis positioner, an interface mounting for receiver, and an extendable truss for orbital deployment of the system.

The initial RF performance calculations indicate that with careful design both candidate configurations could be acceptable even though comparisons were made under somewhat different conditions. However, the mechanical studies show that it is doubtful if the required tolerance could be met in the offset configuration; therefore additional comparison of electrical characteristics was not deemed necessary. The cassegrain configuration was selected and further design studies were conducted.

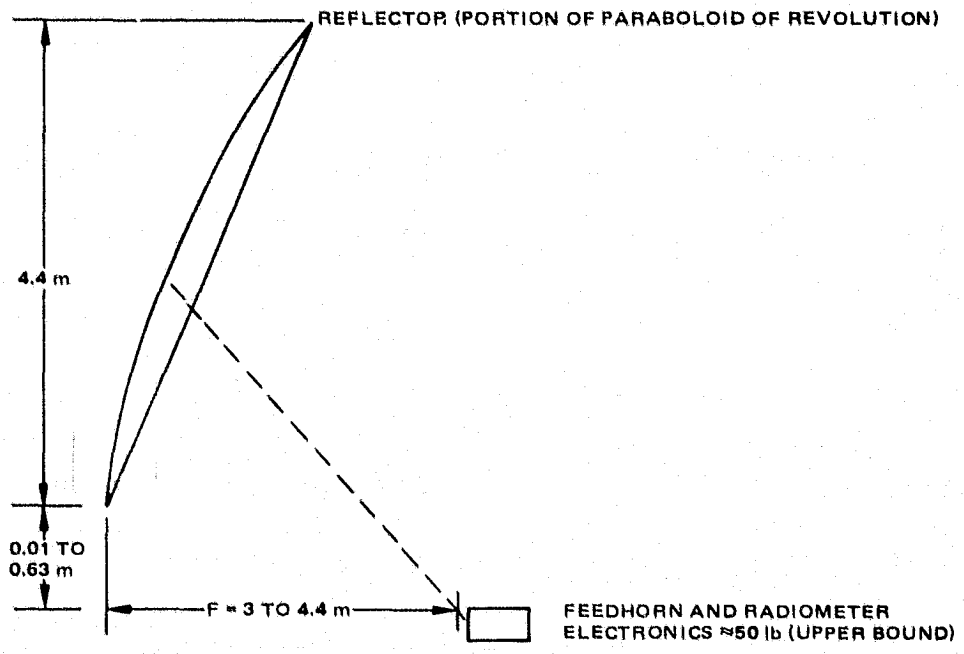

OFFSET PARABOLA

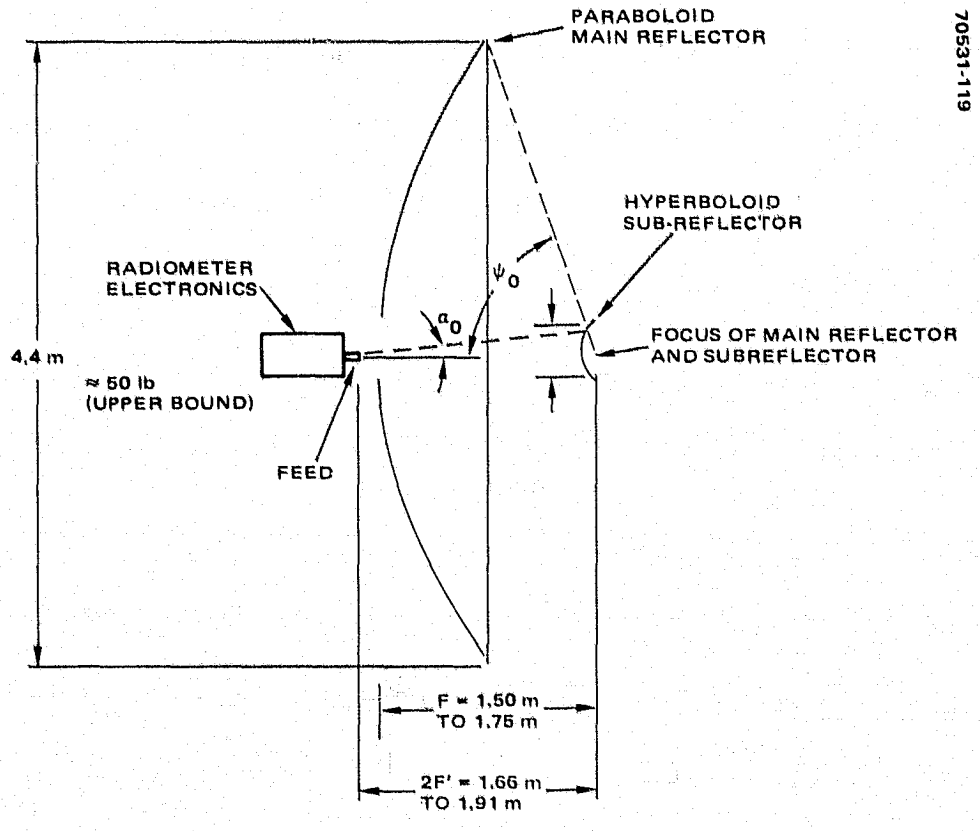

SYMMETRIC CASSEGRAIN

FIGURE 1. PARABOLOIDAL REFLECTOR AND SYMMETRICAL CASSEGRAIN REFLECTOR SYSTEMS

TABLE 1. MECHANICAL DESIGN EVALUATIONS

Parameter	Best Choice	Reason
Weight	Symmetrical cassegrain	Lighter reflector for given aperture diameter
		Lighter support structure with CG behind reflector
		Lighter feed support
Dynamics	Symmetrical cassegrain	Higher natural frequency with deeper shell
		Higher natural frequency with lighter system
Surface tolerance	Symmetrical cassegrain	Easier achievement of surface accuracy with smaller diameter and symmetrical design
Structural	Symmetrical cassegrain	Simpler and more predictable by analysis
Thermal distortion	Symmetrical cassegrain	Reduced distortion with smaller diameter and symmetrical design
		Reduced distortion with closer and symmetrically supported feed
Technical risk	Symmetrical cassegrain	Less risk with experience gained from 8 ft technology program
Cost	Symmetrical cassegrain	Least cost to design and analysis with symmetrical and compact structure
		Least cost for tooling with fewer parts and symmetrical structure; also a smaller PDMO* required
		Least cost for fabrication with fewer parts and symmetrical structure; also most parts identical
		Least cost for contour measurement with symmetrical structure

70531-120T

*Presently, no facilities found to manufacture required single piece PDMO for offset paraboloid.

PDMO = production mold.

TABLE 2. RECOMMENDED ANTENNA CONFIGURATION

Symmetrical cassegrain antenna

- Potentially high beam efficiency and high aperture efficiency
- Stiffer than offset of same weight
- Lower inertia than offset reflector
- Maintains tighter tolerances than offset of same weight
- More cost effective
- Less technical risk

70531-121T

3.2.1 BEAM EFFICIENCIES AND SIDELOBES

Beam efficiencies ≥94.6 percent with sidelobes ≤33 dB are estimated for selected cassegrain configuration.

Pattern and beam efficiency calculations were performed for the cassegrain reflector with a Gaussian beam feed. The diameter of the main reflector was held constant at 4.4 meters with an f/D ratio of 0.35. Two subreflector diameters and three different Gaussian aperture tapers were used.

A subreflector diameter of 19.8 cm places the physical edge of the subreflector on the line of sight from the focus to the edge of the main reflector. This dimension permits a significant amount of forward spillover (1 percent). It could also result in diffraction effects at the edge of the subreflector which could degrade the illumination of the main reflector. Extending the subreflector diameter to 25 cm resulted in a reduction of forward spillover and reduced the illuminating function at the edge of the subreflector by an additional 11.9 dB, thereby reducing diffraction effects. The increased diameter also increases aperture blockage slightly, on the order of 0.6 percent.

The results of the computation are summarized in Table 1. The calculations include the effect of subreflector blockage, forward spillover (assuming the ideal Gaussian beam feed), and diffraction effects caused by the subreflector. Blockage by the subreflector support struts is not included. Strut blockage effects are discussed in Topic 3.2.2. Calculations at 104 GHz indicate that by increasing the subreflector size results in increased antenna efficiency, although the beam efficiency decreased 1.5 percent. It is also evident that increasing the illumination taper will increase beam efficiency at the expense of overall efficiency. An illumination taper of 20 dB has been used as a reasonable compromise value for the baseline design. The effects of tolerances are discussed in Topic 3.3.6.

TABLE 1. CASSEGRAIN ANTENNA CALCULATED PERFORMANCE CHARACTERISTICS

Frequency, GHz	D_{main}, meter	D_{sub}, meter	Taper, dB	Gain, dB	1st Side Lobe, dB	2nd Side Lobe, dB	3rd Side Lobe, dB	3 dB BW, degree	Antenna Effect, η_A	Beam Effect, η_B	$\eta_A\eta_B$
104	4.40	0.198	20	72.03	39.5	35.5	41.5	0.048	0.694	0.992	0.688
104	4.40	0.250	18	72.24	34.0	37.0	37.2	0.047	0.729	0.967	0.705
104	4.40	0.250	20	72.05	39.0	38.5	38.8	0.048	0.697	0.977	0.681
104	4.40	0.250	22	71.83	47.0	39.5	40.6	0.048	0.663	0.983	0.652
118.75	4.40	0.250	20	73.22	36.5	40.5	36.5	0.042	0.700	0.971	0.680
140	4.40	0.250	20	74.59	33.5	33.5	35.9	0.036	0.690	0.946	0.653
140	4.40	0.250	22	74.35	36.2	33.6	35.7	0.036	0.654	0.946	0.619
183	4.40	0.250	20	76.97	36.0	42.5	36.0	0.028	0.698	0.969	0.676

Note: Strut blockage, shadowing, and tolerance effects not included.

70531-122T

3.2.2 APERTURE BLOCKAGE AND SHADOWING

Proper design effort can minimize degradation of performance due to aperture blockage by the subreflector and struts.

The effects of subreflector, strut blockage (Table 1), and shadowing have been estimated for the general case of tapered struts that join the main reflector at some radius ρ_o. In the region $\rho<\rho_o$, the subreflector and struts block the waves traveling outward from the main reflector, while in the region $\rho_o<\rho<D/2$ the struts intercept rays traveling from the subreflector to the main reflector, casting a shadow on the main reflector. Since in this application the transverse dimensions of the struts will be large in terms of wavelength, the blockage and shadowing will be essentially optical in nature.

The power removed from the main beam by blockage and shadowing is scattered elsewhere in space. The blockage and shadowing have been evaluated for various strut diameters, tapers, and ρ_o, and the results are tabulated for a 20 dB taper. It is apparent that minimizing strut size will be an important part of any development program.

TABLE 1. SUBREFLECTOR AND STRUT BLOCKAGE EFFECTS

Strut Diameter, cm		Radius Where Fastened to Main Reflector	Subreflector Blockage Efficiency	Total Blockage Efficiency
At Subreflector	At Main Reflector	Met		
2.54	2.54	2.199	0.984	0.946
2.54	2.54	1.467	0.984	0.929
5.08	5.08	1.467	0.984	0.880
5.08	5.08	2.199	0.984	0.909
7.62	2.54	1.467	0.984	0.870
7.62	2.54	1.150	0.984	0.836
5.08	5.08	1.150	0.984	0.851

70531-123T

3.2.3 EFFECTS OF SURFACE TOLERANCES ON BEAM EFFICIENCY

The effects on antenna performance due to mechanical variations in the antenna surface figure provide an excellent criterion for establishing surface tolerance requirements.

The antenna beam efficiencies given in Topic 3.2.1 are achievable from an antenna with perfect surface figure. In practice, manufacturing tolerances, loading stresses, and thermal effects cause variations in the surface figure which seriously affect antenna performance. Since beam efficiency is an excellent indicator of antenna performance, its value relative to that achievable from a perfect surface is calculated and plotted in Figure 1. It is evident that at 183 GHz the rms surface tolerance must be kept small. For example, the relative beam efficiency for a 1.7 mil rms tolerance is 0.916. This degradation factor must be multiplied with the zero error beam efficiency to obtain the overall beam efficiency. If an overall beam efficiency of 0.85 is required, then the zero error antenna beam efficiency must be 0.93 or greater.

Achieving these tolerances is only partly limited by the fabrication process. Existing machines can easily meet the requirements, but the difficulty is in reading, monitoring, and testing the surface figure. Assuming new methods will be devised to perform surface sensing function, then feasibility of meeting the requirements is assured.

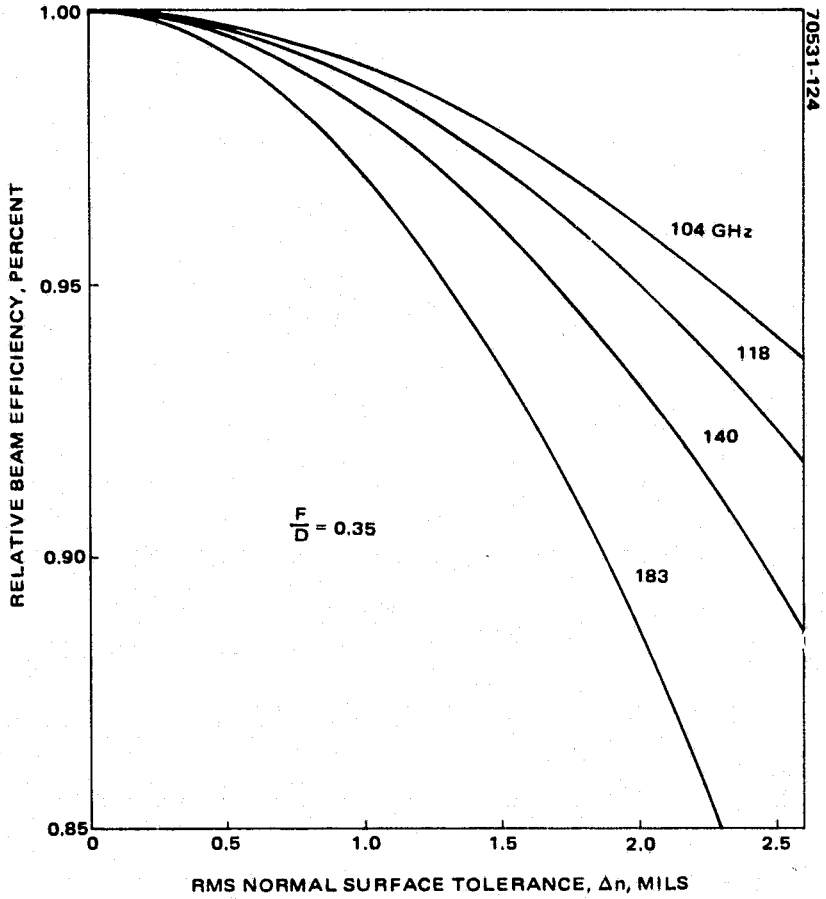

FIGURE 1. EFFECT OF NORMAL SURFACE TOLERANCES ON BEAM EFFICIENCY

3.3.1 BASIS OF APPROACH

The mechanical and thermal design basis of the 4.4 meter MASR antenna are two graphite/epoxy cassegrain antennas - a 2.4 meter and a 3.9 meter detail designs.

Current advanced antenna designs for large, highly precise spaceborne antennas have used graphite/epoxy composites to achieve lightweight, high stiffness, and low thermal expansions. An 8 foot diameter (2.4 meter) technology antenna has been developed and extensively tested which lends confidence to the basic structural techniques. Table 1 lists the design characteristics of the 2.4 meter antenna and compares it with an advanced 3.9 meter design and the 4.4 meter design proposed for MASR. A photograph and performance/construction data of the 2.4 meter antenna are shown in Figure 1.

The structure of the 3.9 meter antenna is illustrated in Figure 2. The main reflector design is based on an f/D ratio of 0.3. The reflector shell is ring stiffened and supported by 12 equally spaced truss ribs that radiate outward from a central torque box. An aluminum alloy subreflector, 15 inches in diameter, is located 41.8 inches above the main reflector vertex. The subreflector is supported from the main reflector structure by four equally spaced struts. A Kapton tent is installed over the back of the antenna to provide a thermal shield for the structure. The tent extends from the rim of the main reflector to the center torque box. Three equally spaced interface fittings are installed at the outer web of the torque box. The overall depth of the antenna from the top of the subreflector structure to the interface attachment plane is 50 inches. All enclosed areas, such as the torque box structure and the shell stiffening rings, are vented.

TABLE 1. COMPARISON OF 2.4, 3.9, AND 4.4 METER DESIGN ANTENNAS

	2.4 Meter Antenna	3.9 Meter Antenna	4.4 Meter Antenna
Weight	45 lb (actual) 20.5 kg	97 lb (calculated) 44.1 kg	125 lb (calculated) 56.8 kg
Reflector Element			
Skin thick, in.	0.032	0.030	0.030
Number of ribs	8	12	12
Rib depth, in.	13	10	23
Number of rings	3	6	5
Natural Frequency, Hz	55	41.5	72.1
f/D	0.3	0.3	0.35
ΔT Across Diameter, °F	+5° to -285°F	+15° to -295°F	+40° to -300°F
Surface Access, mil			
Manufacture	2.5 (actual)	1.2	1.2
Operational	3.1 (actual)	2.0	1.7
Applied Load (Axial)	30 g (actual)	4 g	4 g

70531-125T

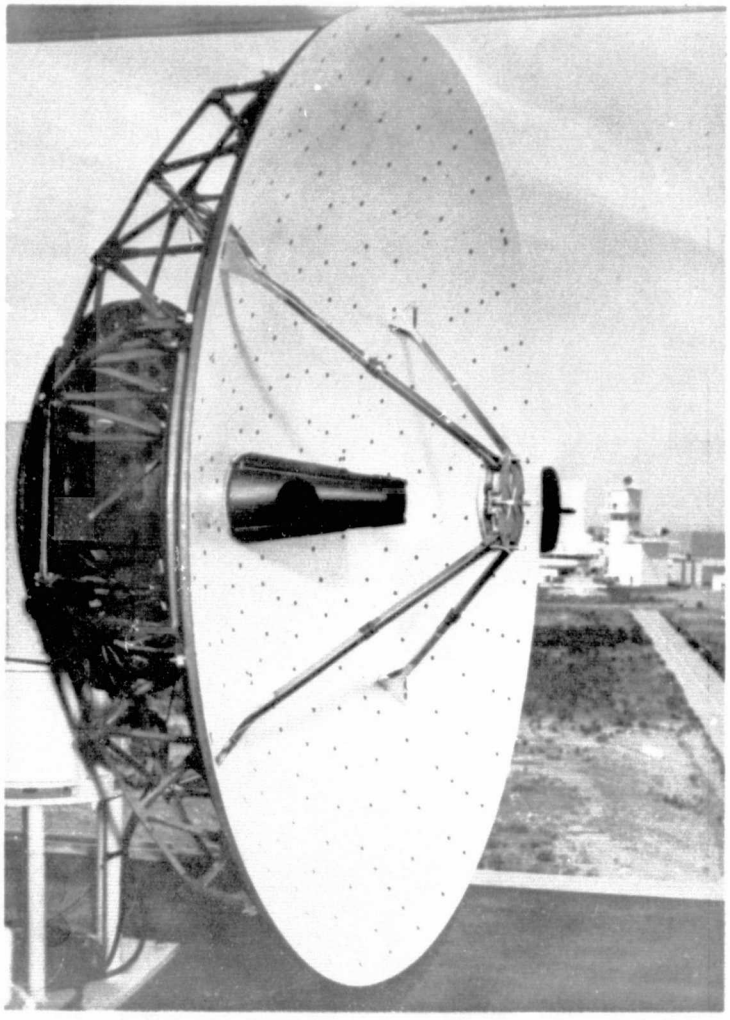

OVERALL CAPABILITIES OF EIGHT-FOOT-DIAMETER TECHNOLOGY ANTENNA.

70531-126

C-BAND TO 300 GHz FREQUENCY COMMUNICATION ANTENNAS ARE FEASIBLE WITH GAIN CAPABILITY TO 70 dB

● RF PERFORMANCE	
GAIN (CAPABILITY), dB	–
1st SIDELOBE, dB	<19
AXIAL RATIO, dB	<0.5
VSWR	<1.1:1.0
BORESIGHT SHIFT, deg	<0.02
TRACKING NULL, dB	>35
● AUTOTRACK CAPABILITY	
MAXIMUM ERROR, deg	0.0071
● MECHANICAL PERFORMANCE	
NATURAL FREQUENCY, Hz	55
INERTIA LOADING, g	30
SURFACE CONTOUR:	
MFG., in	0.0025
ORBITAL, in	0.0031
WEIGHT, lb	45
ACOUSTICS, dB	147
● THERMAL COATINGS	
ABSORPTANCE/EMITTANCE	0.7
SOFT X-RAY, cal/cm^2	0.5
HARD X-RAY, cal/cm^2	2.5
LIFE, yr	7

FIGURE 1. 2.4 METER GRAPHITE/EPOXY CASSEGRAIN ANTENNA

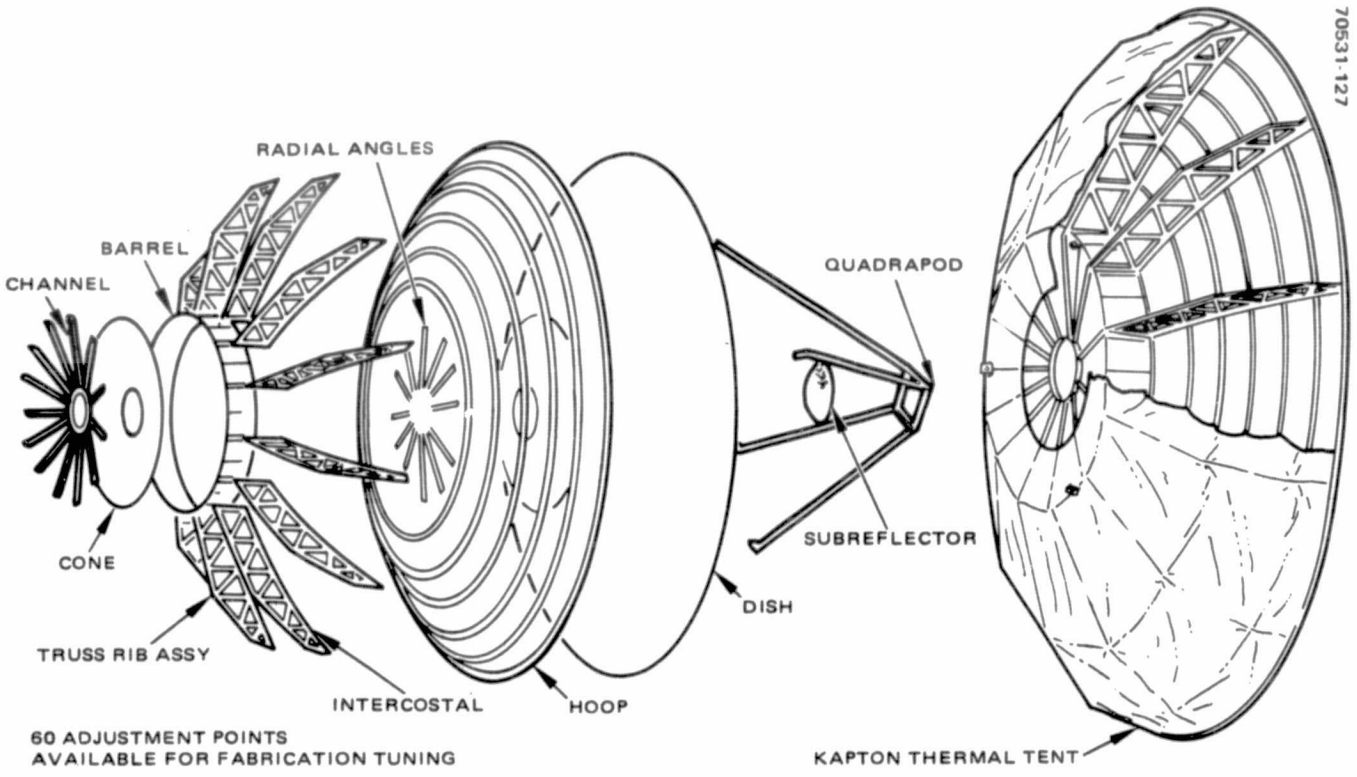

FIGURE 2. 3.9 METER REFLECTOR DESIGN ANTENNA

3.3.2 MATERIAL TRADEOFFS

A figure of merit comparison of materials show graphite/epoxy to be far superior to other materials for the spaceborne 4.4 meter antenna.

Key factors in the selection of the antenna structural material are a low coefficient of expansion (α) and specific weight (ρ), a high Young's modulus (E), and ultimate tensile strength F_{tu}. These factors vary from material to material. Typical values of candidate materials are presented in Table 1.

The structural efficiency of a material is commonly measured by means of a merit function figure of merit obtained by dividing the materials modulus by the product of its specific weight and expansion coefficient. Thus, a high merit function characterizes a material with high stiffness and low weight which is thermally stable. The merit functions of various materials have been computed and are compared in Figure 1. An examination of this figure will show that graphite/epoxy is far superior to other materials for our application.

The strength-to-weight ratio of the candidate materials has also been computed. Unidirectional graphite/epoxy again is shown to be the better material. The strength-to-weight ratio of isotropic graphite/epoxy is about twice that of magnesium and about half that of aluminum.

TABLE 1. MATERIAL COMPARISON

Material	ρ lb/in^3	E lb/in^2 x 10^6	F_{tu} lb/in^2 x 10^3	α in./in°F x 10^{-6}
G/E (undirectional)	0.064	40.0	80	-0.51
G/E (isotropic)	0.064	15.0	28	-0.03
Magnesium	0.064	6.5	15	14.00
Beryllium	0.066	43.5	69	6.00
Boron aluminum	0.096	18.0	76	3.20
Aluminum	0.100	10.0	77	13.00
Titanium	0.160	16.0	134	5.30
Cres. steel	0.286	29.0	30	8.80
Invar	0.295	21.0	32	0.70

70531-128T

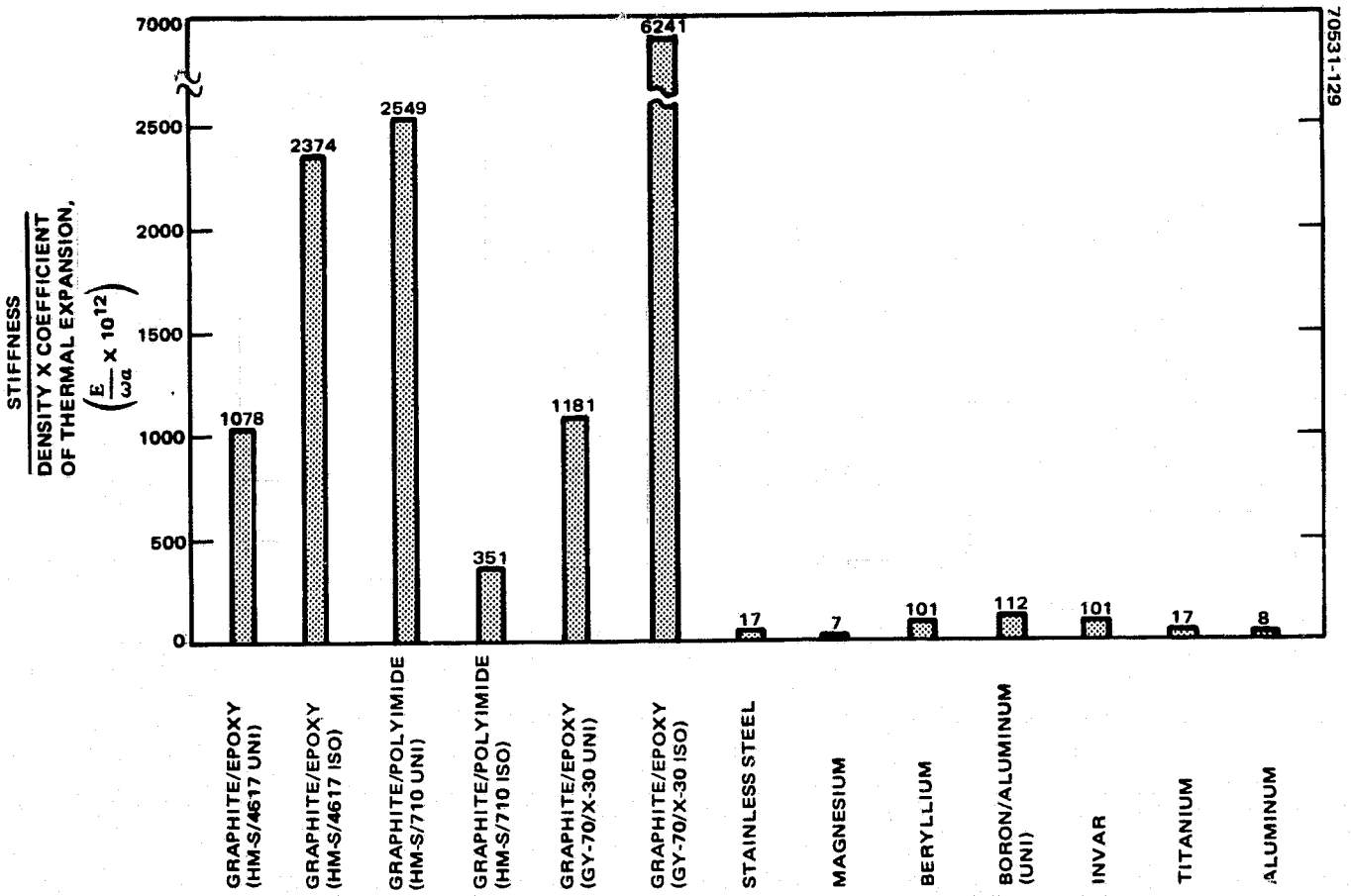

FIGURE 1. MERIT FUNCTIONS OF VARIOUS MATERIALS

3.3.3 SUPPORT STRUCTURE TRADEOFFS

Four concepts of supporting arrangements for the 4.4 meter antenna were evaluated. The support with a collapsible yoke (Concept 4) is the lightest of those considered.

Concept 1. A determinate support at the back of the reflector torque is proposed in this concept (Figure 1a). With a fixed attachment at the back of the reflector, the antenna must pivot about the base of the support. This is a lightweight approach because of the direct tie between the reflector and the spacecraft, but the inertia during E-W axis scan is very large and may not be acceptable. The thermal distortion induced by this support design is minimal.

Concept 2. This partial yoke and beam concept (Figure 1b) eliminates the large inertia effect due to E-W axis scan, but because of its point of mount to the reflector, it could possibly induce thermal distortion. This is also determinate mounting arrangement, provided that a scan mechanism is connected to one side only and the yoke is free floating on the other side.

Concept 3. A nearly full yoke is employed for Concept 3 as depicted in Figure 1c. The intent is to get the support in close to the reflector. Thermal distortion effects are again a possibility as in Concept 2. The separate gimbal points minimize the inertia effects due to scan.

Concept 4. The weights of the prior support concepts are definitely greater than the 10 to 15 pounds necessary to maintain weight within the 250 pound maximum goal for the antenna system. This deployable support concept (Figure 1d) would offer the best chance of meeting the weight constraints (goals). A stiff and high strength support structure to withstand launch loads is not required because of the reduced moments created when the structure is stowed close to the spacecraft during launch.

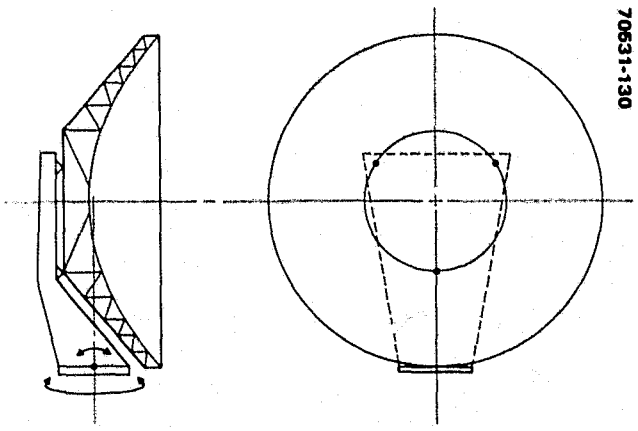

DESCRIPTION:

- SYMMETRICAL CASSEGRAIN – RING/RADIAL BACKUP STRUCTURE
- DETERMINATE SUPPORT AT BACK OF TORQUE BOX
- TAPERED BEAM SUPPORT
- COMBINED GIMBAL LOCATION

a) CONCEPT 1

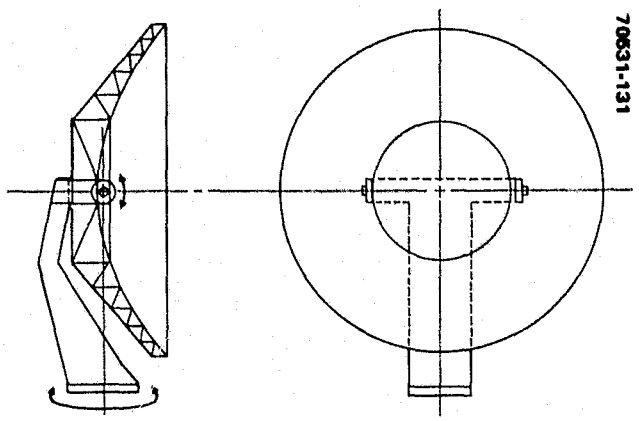

DESCRIPTION:

- SYMMETRICAL CASSEGRAIN – RING/RADIAL BACKUP STRUCTURE
- DETERMINATE SUPPORT AT SIDE OF TORQUE BOX
- YOKE AND STRAIGHT BEAM SUPPORT
- SEPARATE GIMBAL LOCATIONS

b) CONCEPT 2

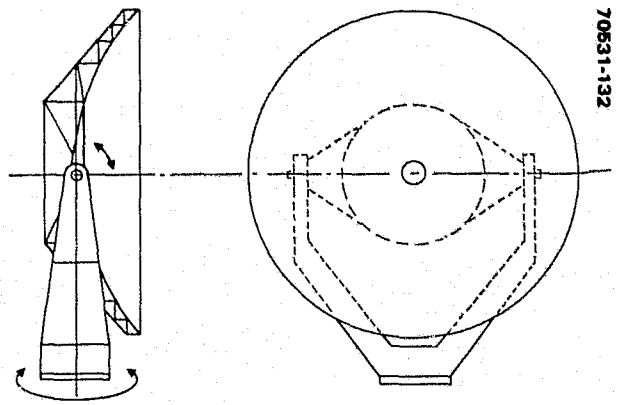

DESCRIPTION:

- SYMMETRICAL CASSEGRAIN – RING/RADIAL BACKUP STRUCTURE
- DETERMINATE SUPPORT AT SIDE OF TORQUE BOX
- FULL YOKE SUPPORT
- SEPARATE GIMBAL LOCATIONS

c) CONCEPT 3

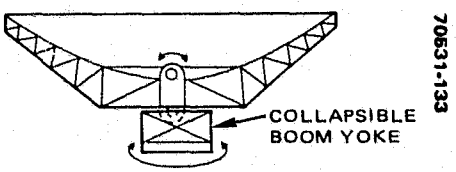

DESCRIPTION:

- SYMMETRICAL CASSEGRAIN – RING/RADIAL BACKUP STRUCTURE
- DETERMINATE SUPPORT AT SIDE OF TORQUE BOX
- COLLAPSIBLE BOOM/YOKE SUPPORT
- SEPARATE GIMBAL LOCATIONS

d) CONCEPT 4

FIGURE 1. ANTENNA SUPPORT STRUCTURES

3.3.4 BASELINE DESIGN AND DEPLOYMENT SEQUENCE

Lightweight and caged mounting during launch favor the selection of the collapsible yoke baseline design.

Baseline Design Description. The selected baseline configuration (Figure 1) is a cassegrainian with a primary f/D ratio of 0.35. The paraboloidal primary reflector is a 4.4 meter diameter while the aluminum secondary (subreflector) is 25 cm diameter. The RF feed is located close behind the primary reflector vertex and is contained within the 0.60 meter diameter radiometer module. The antenna is mechanically scanned in rastor fashion using a two axis gimbal system.

In order to meet the stringent thermal stability and dynamic stiffness requirements, the selected structural material for the reflector assembly is GY-70/X-30 graphite/epoxy, pseudoisotropic laminate. For the adapter and support frame where structural stiffness is more critical than thermal stability, the laminate for the structural elements is more predominantly unidirectional.

Deployment Sequence. In the stowed position, the antenna rests on six secondary support struts that provide support during the boost phase (Figure 2a), which then disconnect and retract to permit in-space deployment of the antenna system.

The support frame deploys from its stowed location (Figure 2b) by rotating its two space frames to achieve the deployed (operational) configuration shown in Figure 2c. As illustrated in Figure 2, the support frame has been configured to fit the STORMSAT geometry.

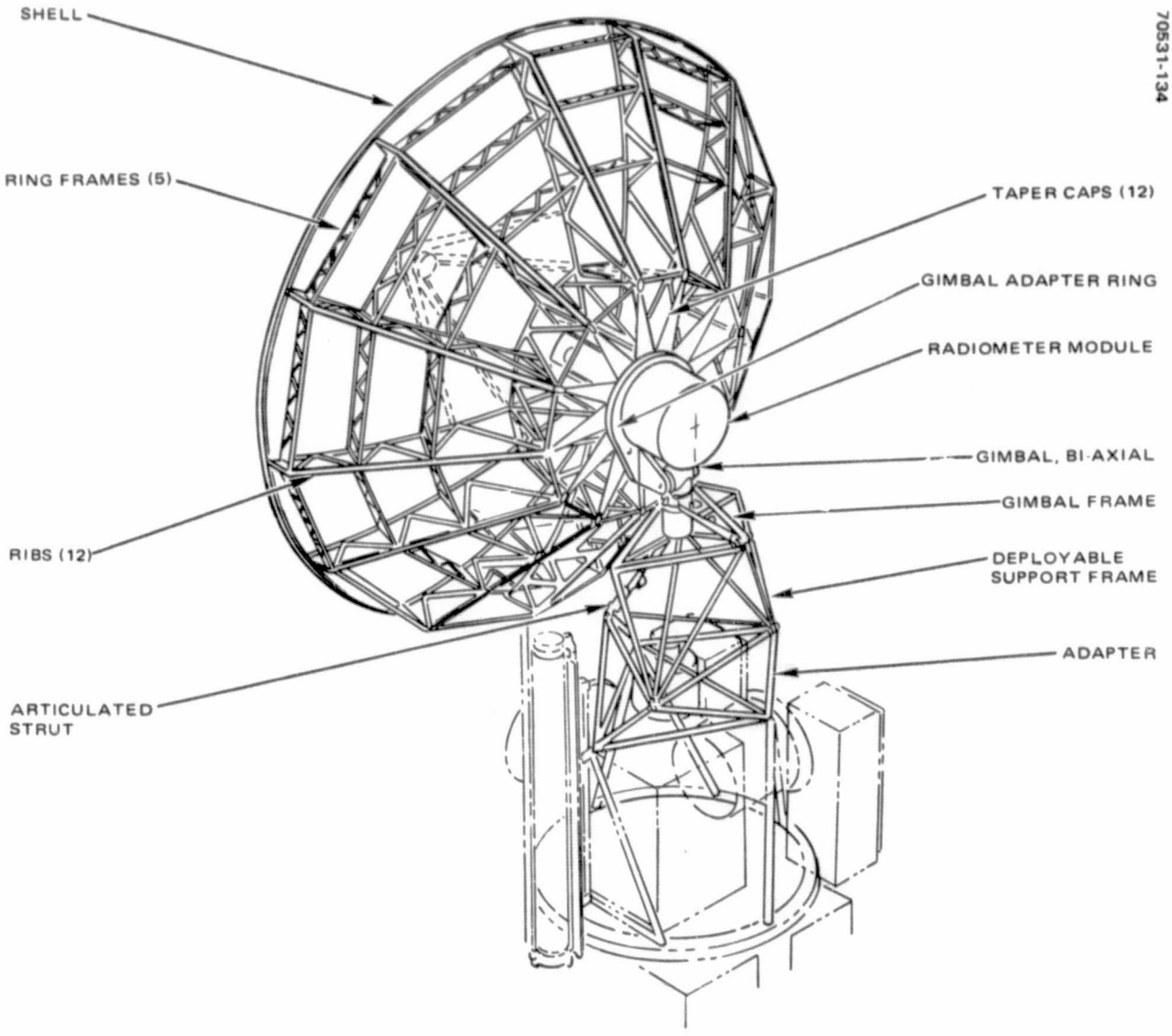

FIGURE 1. MASR BASELINE ANTENNA SYSTEM

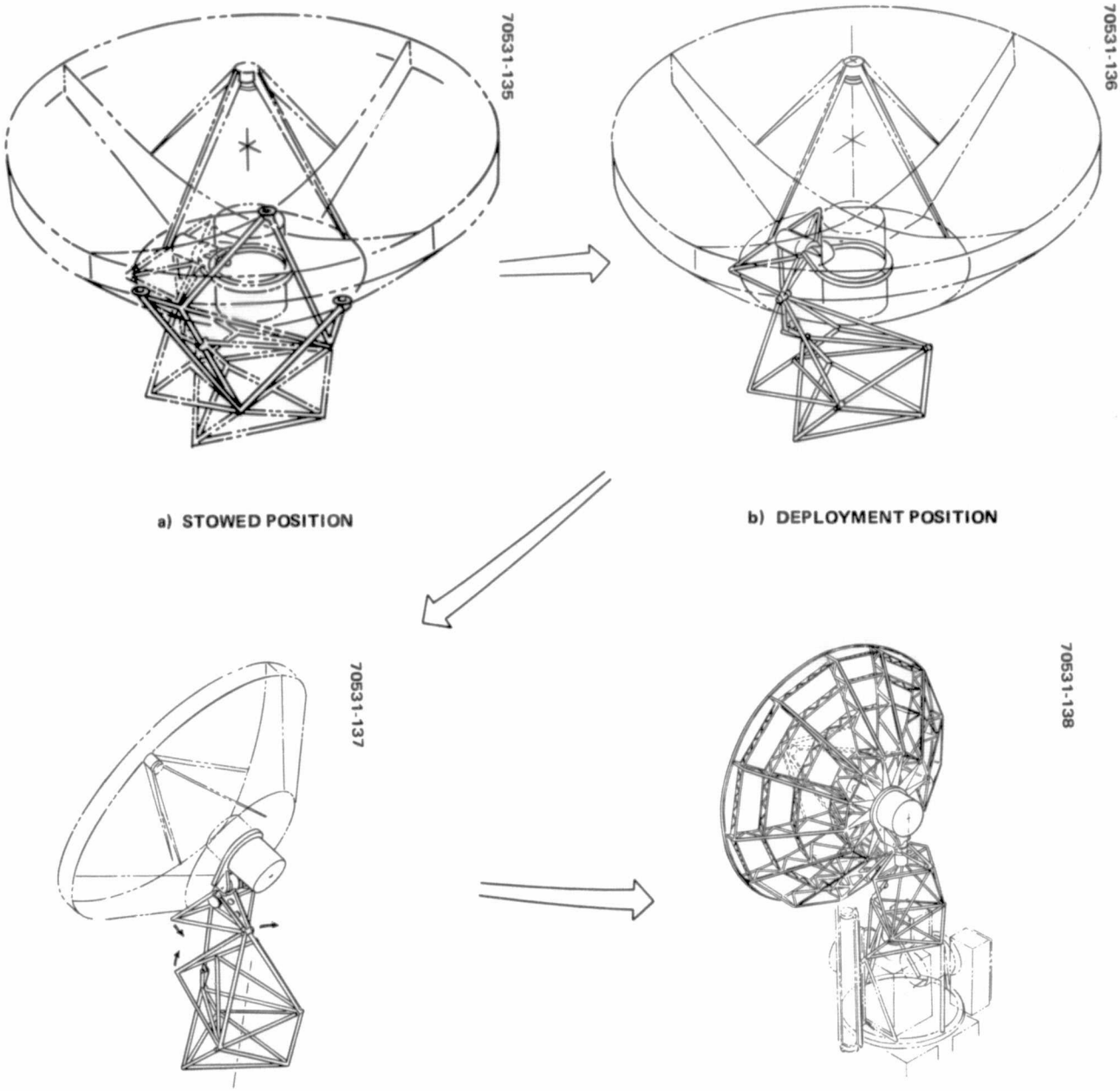

FIGURE 2. 4.4 METER ANTENNA DEPLOYMENT SEQUENCE

PRECEDING PAGE BLANK NOT FILMED

3.3.5 STRESS ANALYSIS

The SOLID SAP program dynamic thermal-mechanical analysis has confirmed the spaceworthiness of the MASR antenna.

Antenna Dish. The preliminary stress analysis of the 4.4 meter MASR antenna has proven the feasibility of successfully meeting the structural performance criteria proposed for the system. The primary areas of consideration for this study are the dynamic and thermal characteristics and the structural integrity of the antenna dish structure and support tower. Several finite element models using Convair's SOLID SAP program were generated to perform the analyses.

Deployable Support Frame. The support structure for the antenna during in-orbit operation is modeled separately from the dish. The two models can be analyzed separately because the natural frequencies are widely spaced to avoid coupling. The mass and the mass moments of inertia of moving portions of the antenna structure are modeled as lump masses at the component centers of gravity. This eliminates the problems of cross coupling terms of translation and rotation.

Table 1 highlights the STORMSAT antenna structural system.

TABLE 1. STORMSAT ANTENNA STRUCTURAL SYSTEM

Antenna Dish
• Dynamics
• Thermal distortion
• 1 g gravity
• Structural integrity
Support Structure — In Orbit
• Dynamics
• Structural integrity
Caging Structure — Launch
• Structural integrity

70531-139T

3.3.6 MAJOR ASSUMPTIONS AND FINDINGS OF STUDY

It is feasible to achieve a deployable 4.4 meter symmetrical cassegrain antenna in a space package with 200 pounds combined reflector and support structure weight (Table 1), with an rms surface tolerance of 1.7 mils (Table 2).

TABLE 1. WEIGHT ALLOCATION SUMMARY FOR 200 lb COMBINED REFLECTOR/SUPPORT STRUCTURE

	Pounds
Reflector and backup structure	125
Thermal blanket	8
Gimbal attachment mount	16
Deployable frame support	43
Launch support structure	8
Total	200

70531-140T

TABLE 2. SURFACE TOLERANCES

	Budget, mil
Tool manufacturing	1.20
Adjustment error	0.20
Thermal distortion	0.48
Subreflector	0.30
1 g sag (max condition)	0.06
Slew error	0.01
Moisture absorption (allowance)	1.04
Total rms (root sum of squares rss)	1.70

70531-141T

Notes:

1) One piece skin, both producible and adjustable, to meet operational surface accuracies.

2) Surface accuracy error budget, rms.

3.4 RECOMMENDED FURTHER STUDY

To reduce the cost/schedule risk of antenna development for a potential flight program, further studies of antenna development and testing methods are recommended.

Antenna Testing Methods. The testing of a large millimeter wave antenna poses some difficult problems. Direct measurements of patterns and gain require antenna ranges with long paths. Even if they were available, atmospheric effects such as attenuation and scintillation would make accurate measurements difficult. Other techniques such as near field techniques require large, precise equipment and facilities. A more detailed study of testing techniques and the measurement accuracies attainable with each is necessary to estimate costs, schedules, and achievable accuracies.

Feed Studies. A second area in which additional preliminary study is desirable is the interaction of the quasi-optical feed technique with the cassegrain reflector. Effects such as the consequences of the limitation of beam transverse dimensions and the departure from true Gaussian shape must be considered, since these effects have an impact on forward spillover loss and ultimately, on the calibration temperature of the antenna.

Reflectivity Measurements. A third area where more data are required is that of the reflection coefficients of aluminum and dielectric coatings. Measurements of these quantities should be made over the frequency range of interest.

Eight Foot Antenna Model. It is recommended that a new 8 foot technology antenna be designed, fabricated, and tested. This is necessary to utilize state of the art technology and new materials technology to demonstrate the feasibility of a scaled down 4.4 meter MASR antenna reflector. Accuracies for the scaled down reflector would necessarily be more stringent.

Materials Development. The GY-70/X-30 material proves to be the best choice for the MASR antenna because of its high stiffness and thermal stability over a wide range of temperature. Even so, it is questionable whether GY-70/X-30 will be thermally stable enough to satisfy surface accuracy (rms) requirements during space operation because of the extreme temperature range expected for the MASR antenna (-300°F to +100°F). Microcracking has been shown to occur at temperatures below -150°F in the GY-70/X-30 laminate, which with repeated cycling, drives the CTE of the laminate to a value of -0.5×10^{-6} in/in°F, severely affecting the accuracy of the reflector surface. Interestingly enough, other graphite/epoxy combinations (i.e., HMS/934, T-300/934) which may be unacceptable because of initially high CTE ($+0.7 \times 10^{-6}$) could microcrack and have a tolerable CTE. The uncertainties about microcracking relative to the temperatures at which microcracking will occur, effects of cycling, processing effects, and many others suggest further material testing.

Consideration should also be given to investigating laminates which seem to be less prone to microcracking, and hybrid laminates that resist microcracking, or to optimization of a laminate (regardless of microcracking presence in the laminate).

Moisture Absorption. Another materials related problem is moisture absorption. It is expected that surface accuracy (distortion) will be affected by the existence of moisture in the graphite/epoxy material. The effect moisture absorption has on accuracy is very difficult to assess:

1. Parts of the reflector may have varying degrees of moisture present at launch and subsequently lose the moisture at varying rates. Temperature gradients across the reflector can affect the desorption rate.

2. The basic reflector skin and backup structure interface design may influence the effect moisture absorption/desorption has on surface distortion.

3. Environmental control procedures that are reasonable to expect for the MASR antenna are not known at this time.

4. The combination of microcracking and moisture absorption on the surface accuracy can produce opposite or balancing effects.

It is recommended that further moisture testing on graphite/epoxy laminate be pursued.